Chemical Engineering Journal Advances 23 (2025) 100789

Contents lists available at ScienceDirect

Chemical Engineering Journal Advances

journal homepage: www.sciencedirect.com/journal/chemical-engineering-journal-advances

Dynamic PCM strategies with nano-enhanced composites for optimal thermal energy storage and management

Amit Kumar Mishra [a], Matteo Morciano [a], Biruk Wondifraw Agegnehu [a], Elena Campagnoli [a], Valter Giaretto [a], Andrea Bottega [a], Matteo Fasano [a], Luigi Mongibello [c], Eliodoro Chiavazzo [a,b,*]

[a] Department of Energy, Politecnico di Torino, Corso Duca degli Abruzzi 24, Torino 10129, Italy
[b] Istituto Nazionale di Ricerca Metrologica, Strada Delle Cacce 91, Torino 10135, Italy
[c] Enea Portici, P.le Enrico Fermi, 1 - Località Granatello, Portici (Na) 80055, Italy

ARTICLE INFO

Keywords:
Latent thermal energy storage
Dynamic PCM
Nanocomposite PCMs
Heat transfer enhancement
Power density
Thermal management
Solar energy harvesting

ABSTRACT

We demonstrated the role of dynamic phase change materials (dynamic PCM) and nanofiller characteristics in the effective improvement of thermal energy storage (TES) and management performance. This is the very first study where nano-enhanced PCMs have been tested in a dynPCM configuration and compared the heat storage potential with respect to pristine PCM. We investigated the influence of nanofiller characteristics on the effective thermophysical properties of composite PCMs. To this end, we report a remarkable enhancement in thermal conductivity (~76 %) in lauric acid-based composite PCMs loaded with 4 wt. % graphene nanoplatelets (GNP) and carbon black (CBNP) concentrations. Those improvements are known to be attributed to the ability of nanofillers to establish efficient heat transfer by percolating network structures. We illustrated dynPCM is an effective approach to control the melt-front thickness (δ) and thus interface thermal resistance, which significantly improves power density for the latent TES system, and may benefit from the presence of PCM nanocomposites. Recently, PCMs have also shown promising potential for direct solar energy harvesting. Notably, GNP-based composite PCMs can be used for superior solar thermoelectric performance (enhanced output voltage ~ 36 %) compared to pristine PCMs, resulting from the synergistic effects of improved heat conduction and photothermal conversion. This work presents robust experimental findings highlighting the potential of nanocomposite PCMs and dynPCM in advancing TES and solar energy harvesting technologies.

1. Introduction

Rising energy consumption and environmental concerns emphasize the significance of advanced energy storage and conversion technologies [1–3]. Clean energy harvesting from the sun and waste heat holds great potential to address environmental challenges and energy scarcity [4–6]. Among various methods, thermal energy storage (TES) technologies emerge as a prime approach to overcome the above issues, since they allow to balance energy supply and demand, thus lowering carbon emissions [7–10]. Additionally, photothermal energy conversion and storage systems have also generated widespread interest due to their cost-effectiveness and efficiency [11,12].

Apart from energy-saving and utilisation concerns, effective thermal management of high heat flux from electronic devices also requires more effective solutions to prevent overheating, which can potentially degrade their working efficiency and operating life [13–15]. For these applications, latent TES systems using phase change materials (PCMs) are an attractive choice due to their high energy density (2–3 times compared to sensible heat storage systems), low cost, reduced environmental impact, and capability to store and release thermal energy at a nearly constant temperature, corresponding to the phase transition temperature of the PCM [16,17].

PCMs have been extensively used in various fields, such as solar heat storage, energy-saving buildings, waste heat recycling, thermal management of electronics, and thermoelectric generators [18–21]. PCMs-based TES systems exhibit high energy density, tuneable phase change temperature, and thermal stability, with a demonstrated potential for helping accomplish sustainable development goals and net

* Corresponding author.
E-mail address: eliodoro.chiavazzo@polito.it (E. Chiavazzo).

https://doi.org/10.1016/j.ceja.2025.100789

Available online 10 June 2025

Table 1
Description of materials' suppliers and features.

Name	Source	Purity	Dimensions	Specific surface area (m^2/g)
Lauric acid (LA)	Sigma-Aldrich	~ 99 %	–	–
Carbon black nanoparticles (CBNP)	PowderNano	~98 %	Size ~20 nm	~195
Graphene nanoplatelets (GNP)	Ossila Ltd.	~ 99.9 %	Size ~1.5 μm Thickness ~3 nm	~800

zero emissions [22,23]. In particular, lauric acid (LA) is a widely adopted PCM due to its solid-liquid phase change at relatively low temperature (~ 45 °C), high latent heat, no-supercooling, non--corrosiveness, no-phase-separation, and good chemical and thermal stability. These characteristics make LA an excellent candidate for various low-temperature applications of PCMs [21,24]. Still, the practical applicability of organic PCMs is severely limited due to some poor physical properties, among which thermal conductivity (TC) and photo-thermal conversion (PTC) rate, which directly affect their performance in energy applications [25–27]. Low TC leads to slow charging/discharging transients during phase change processes, whereas poor light absorption causes low PTC efficiency. Therefore, investigation, study and use of composite PCMs exhibiting enhanced heat conduction and sunlight absorption have attracted attention for thermal storage, management and solar energy harvesting [28,29].

In the past, several attempts have been made to design nanocomposite PCMs to overcome the typical drawbacks of pristine PCMs. Through these efforts, it has been demonstrated that the incorporation of nanofillers significantly helps to improve the heat conduction and PTC performance of PCMs [30–32]. Various carbon and metal-based nanofillers effectively boosted the TC and PTC performance of composite organic PCM, e.g., graphene nanoplatelets [33,34], carbon nanotube [35,36], carbon foams [37], expanded graphite [38],

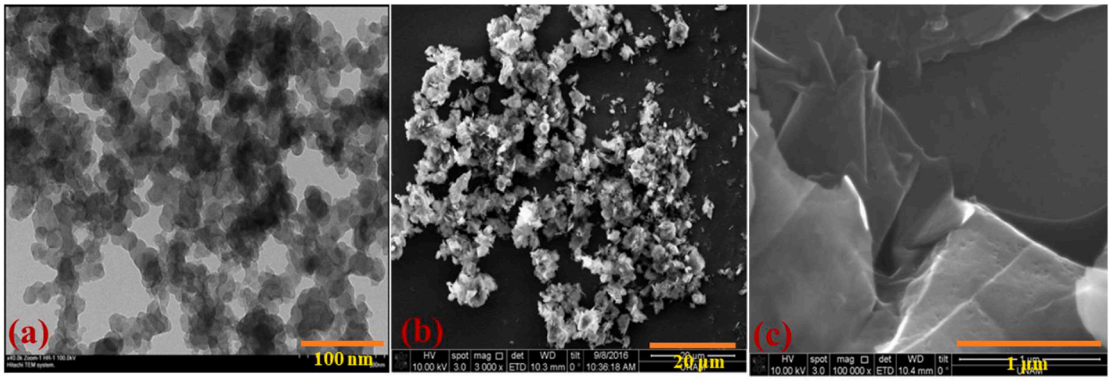

Fig. 1. TEM images of (a) carbon black nanoparticles (CBNP), and (b)-(c) graphene nanoplatelets (GNP) as provided by PowderNano and Ossila Ltd. suppliers, respectively.

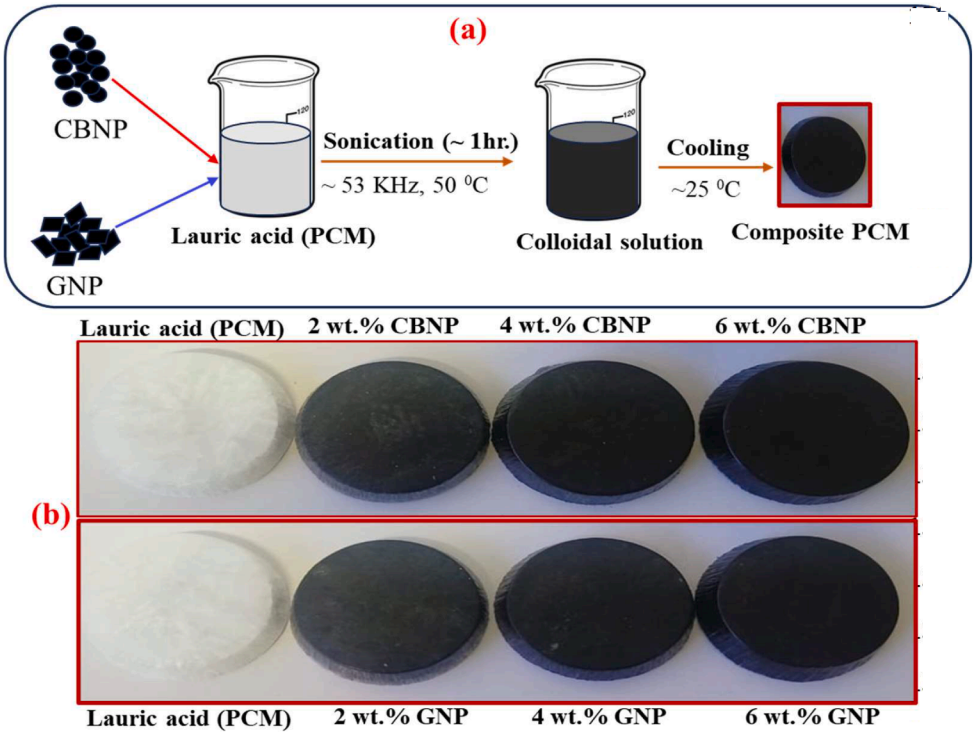

Fig. 2. (a) Illustration of composite PCMs preparation steps. (b) Images of CBNP- and GNP-loaded composite PCMs at different fillers concentrations.

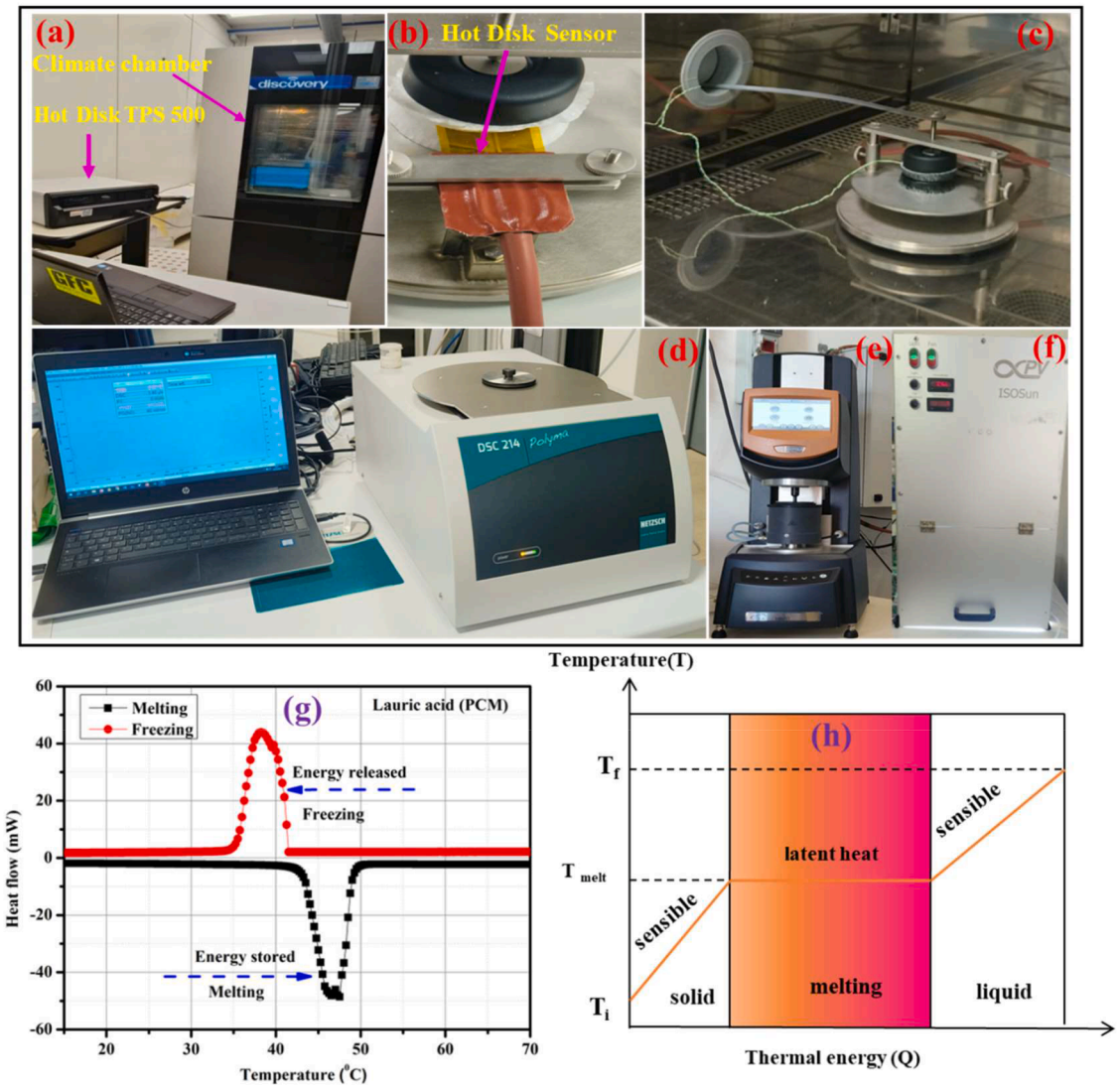

Fig. 3. (a), (b) and (c) show the experimental setup adopted to measure the thermal conductivity (Hot disk TPS 500). (d), (e) and (f) DSC, viscosity and photothermal (simulated sunlight source) measurement tools, respectively. (g) DSC curves of pure PCM. (h) Schematic of TES of typical PCM.

expanded vermiculite [39], boron carbide [40], gold [41], silver [24], copper [42,43], and zinc nanoparticles [44].

Among these, carbon-based fillers are particularly favoured because of their excellent optical and thermo-physical features, such as high thermal conductivity, stable chemical nature, extensive usability, and low density [45–47]. Additionally, carbon-based fillers provide intrinsic high TC and create effective percolation network pathways to enhance heat conduction and optical (light-heat) conversion abilities of composite PCMs through thermal vibration within atomic lattices (excitation of loosely bound π orbitals electrons to π* orbitals) [34,48,49].

Furthermore, under high specific heat flux (e.g., thermal management of electronics [50–52]), the TES performance of PCMs also depends upon the adopted melting approach [53,54], e.g., constrained, gravity-driven, or pressure-enhanced one. In the typical constrained melting, the liquid PCM does not easily flow because of the physical boundaries of the container, leading to reduced heat transfer due to the progressive accumulation of melted PCM and thus growing thermal resistance close to the heating surface. In a second melting strategy, the growth of the melting front thickness over time is mitigated by removing the liquid PCM in a passive way, i.e. exploiting gravity. Finally, the operation of pressure-enhanced PCM (also known as dynamic PCM – dynPCM) [55–57] allows the active removal of the melted phase, therefore further minimizing the interface thermal resistance between the heat source and solid PCM and enhancing the power density of TES.

The addition of nanofillers into the PCM can also enhance the melting performance during the charging process given the higher TC of the composite; however, the concurrent viscosity increase due to nanoparticle addition can suppress natural convection and thus limit heat transfer [58]. Hence, understanding the role of thermophysical characteristics and combining the synergic effects of nano-enhanced and pressure-enhanced PCM strategies could be very promising for achieving heat storage and thermal management with superior performance, especially as far as power density is concerned.

In the present study, we demonstrate the role of nanofiller characteristics and pressure-enhanced PCM on the thermal energy storage and management performance of lauric acid. Specifically, we assess the impact of nanofillers on the enhancement of heat conduction, energy storage, power density and solar thermal energy conversion. To the best of our knowledge, the impact of nanofiller characteristics on the performance of composite PCMs in these areas has not been comprehensively addressed in prior research. Our experimental findings show that composite PCMs loaded with carbon black nanoparticles (CBNP) and graphene nanoplatelets (GNP) exhibit significantly higher heat conduction and photothermal performance compared to pristine PCMs.

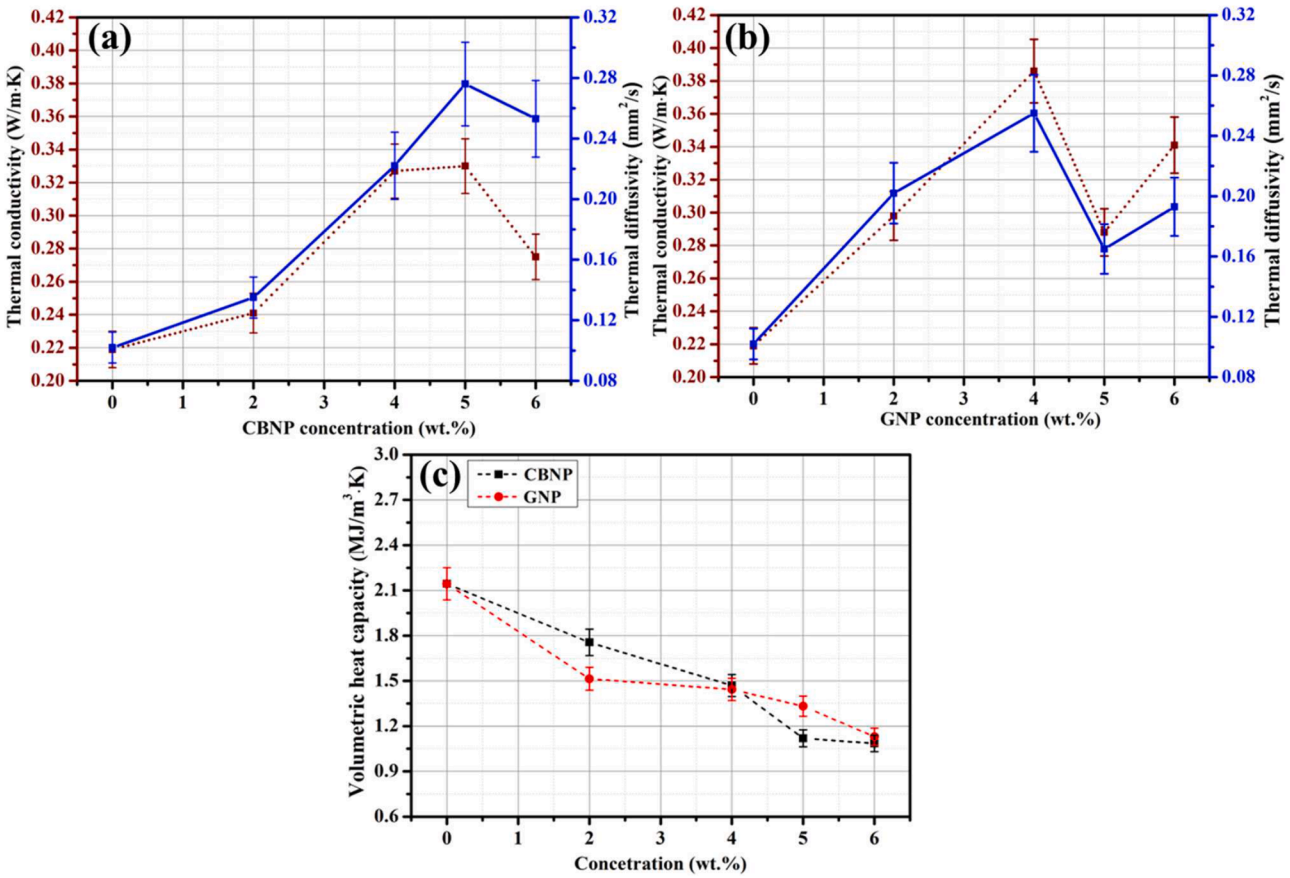

Figs. 4. (a)-(b) Variation in thermal conductivity/diffusivity of composite PCM (solid phase) with loading concentration of CBNP and GNP nanoparticles, respectively. (c) Variation of volumetric heat capacity of composite PCM as a function of filler concentrations.

Furthermore, the morphology, physical properties, and agglomeration of the nanofillers were found to influence the thermophysical properties of composite PCMs strongly. We also provide preliminary evidence that combining composite PCMs with dynPCM can further help improving thermal energy storage and management performance.

2. Materials and experimental methods

2.1. Materials and sample preparation

Lauric acid was purchased from Sigma-Aldrich (99 % purity); the CBNP and GNP were purchased from PowderNano and Ossila Ltd., respectively (see Table 1). The materials received from the suppliers were used without further purification. To understand the role of nanofiller concentrations on thermophysical properties, composite PCMs have been prepared at various loadings of CBNPs and GNPs. The different concentrations (2.0, 4.0, 5.0 and 6 wt. %) of CBNP and GNP nanoparticles were directly dispersed in the liquid PCM (sample temperature higher than corresponding PCM melting point, with bath temperature maintained at 50 °C). Thereafter, the sample was subjected to water bath sonication (~53 kHz), operating at full power for 1 h at sonication intensity ~28 W/L. The resulting mixture was cooled at room temperature and the composite PCMs with various loadings of CBNP & GNP were prepared for thermophysical characterization (cylinders with a diameter of ~ 5.8 cm, height ~1.1 cm). Fig. 1(a) shows a TEM image of CBNPs with discernible particle size ~20 nm, while Figs. 1(b)-(c) TEM images of graphene GNPs demonstrating planar structure and size of GNP flakes ~1.5 μm. The nanofiller-based composite PCMs preparation process and some pictures of the prepared samples are illustrated in Figs. 2(a)-(b).

2.2. Characterization and performance evaluation of composite PCMs

The thermal conductivity and diffusivity of PCM-based samples were determined using a Hot Disk Thermal Constants Analyzer (Hot Disk, TPS 500, see Fig. 3(a)) with a nominal accuracy of ±5 % and ±10 %, respectively. The temperature-dependent study was carried out by using a climate chamber, which helped to precisely control and tune the sample temperature (within ± 1 °C). The hot disk sensor comprises an electrically conducting pattern in the shape of a double spiral, which has been etched out of a thin metal (Nickel) foil. This sensor acts as a heat source for raising the PCM sample's temperature and concurrently recording the temperature changes with time. During measurements, a plane hot disk sensor is fitted between two pieces of the sample and a small constant current is applied; the related working principle and measurement details of the thermal properties analyser (TPS) are available at ref [59].

Figs. 3(b)-(c) show the thermal sensor kept between the pair of specimens and firmly supported by a stainless steel-based chamber while measuring the thermal properties of pristine and composite PCMs. The phase change characteristics and latent heat values of the pristine and composite PCMs were investigated by differential scanning calorimetry (DSC) under a nitrogen (N_2) atmosphere with a 3 °C/min heating rate (DSC 214 Polyma, Fig. 3(d)). The phase transition temperature and latent heat of pristine and composite PCM were obtained with a precision of ± 0.2 %. The dynamic viscosities of liquid samples at ~55 °C were measured using a rheometer (TA Instrument Discovery HR20), employing soak time, shear rate, and sampling interval parameters (180 s, 100.0 1/s, and 1.0 s/pt), respectively, Fig. 3(e).

A solar simulator (infinityPV ISOSun, Fig. 3(f)) was used to mimic a concentrated solar light irradiance (150 mW/cm^2), and the

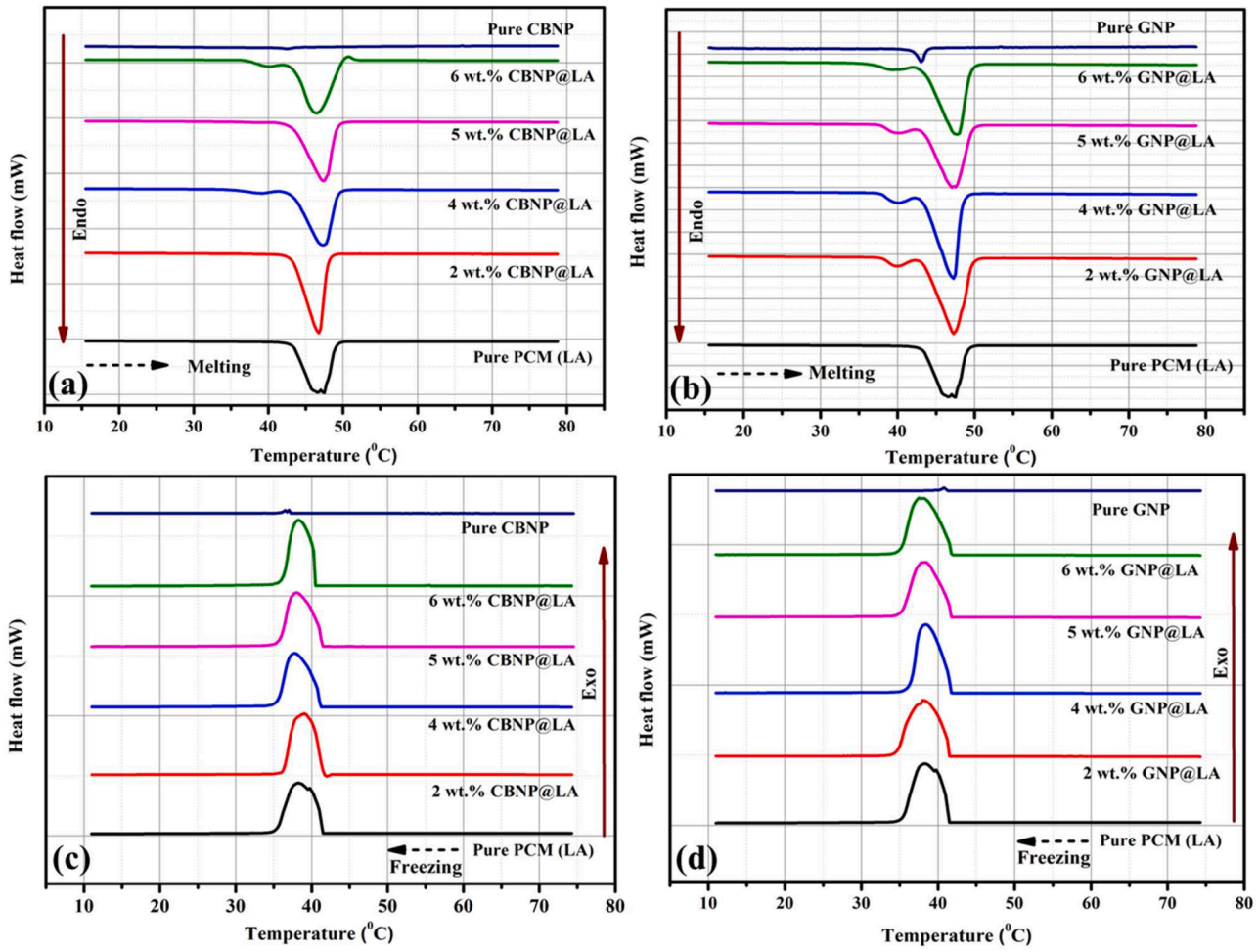

Fig. 5. (a)-(b) DSC curves during melting and (c)-(d) during freezing of various composite PCMs at different loading concentrations of CBNP & GNP. DSC curves of LA (pure PCM) and fillers (CBNP & GNP) are also shown for comparison.

Table 2
Thermal properties of PCM and nanofiller loaded composite PCMs.

Sample	Melting Process			Cooling Process			At ~25 °C
	Melting point (°C) (± 0.1 °C)	(Exp.) Latent heat (J/g) (± 0.4)	(Calc.) Latent heat (J/g)	Freezing point (°C) (± 0.1 °C)	(Exp.) Latent heat (J/g) (± 0.4)	(Calc.) Latent heat (J/g)	c_p (J/g.K) Solid-state
PCM(LA)	45.4	172.5	172.5	40.1	170.4	170.4	2.03
2 wt. % CBNP	44.8	170.5	169.6	40.2	165.5	167.0	2.13
4 wt. % CBNP	44.4	163.2	165.7	39.9	162.8	163.5	1.97
5 wt. % CBNP	44.5	160.1	163.9	40.0	158.4	161.8	1.74
6 wt. % CBNP	44.7	158.2	162.1	40.1	157.2	160.2	1.37
2 wt. % GNP	44.8	168.5	169.6	40.2	167.5	167.0	1.92
4 wt. % GNP	44.5	163.2	165.7	40.1	160.8	163.5	1.76
5 wt. % GNP	44.8	157.1	163.9	40.0	155.4	161.8	1.70
6 wt. % GNP	44.7	152.2	162.1	40.1	151.3	160.2	1.54

photothermal conversion performance was studied by measuring the sample's temperature variation using K-type thermocouples (recording data every second with uncertainty of ~2 %). The investigation of the solar-thermal-electric conversion performance of pristine and composite PCMs was done through the design of a solar thermoelectric setup with the help of a commercially available thermoelectric generator (TEG) module (5.5 cm × 5.5 cm). The target PCM sample was irradiated by the solar simulator, and the generated heat transferred to the hot end of TEG chip while connecting the cold end to an aluminium heat sink at ~21 °C (Fig. 13(b)). A digital multimeter was used to monitor the open-circuit

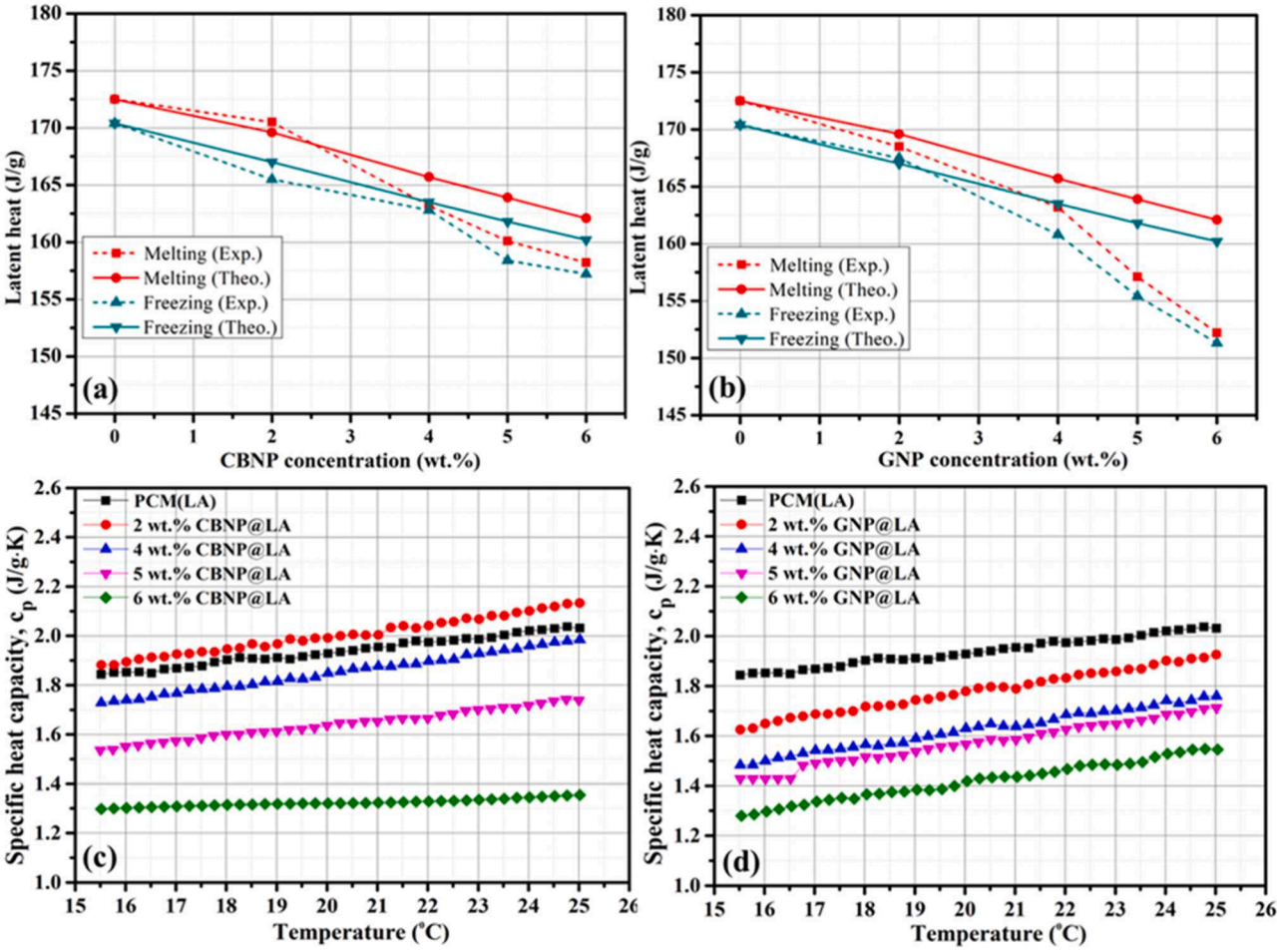

Fig. 6. (a)-(b) Variations of experimental and theoretically calculated latent heat values during the melting and freezing process. (c)-(d) Variation of specific heat capacity (c_p) as a function of temperature (in solid state) at different loadings of composite PCMs.

voltage of the thermoelectric module with uncertainty of ~ 3 %.

The improvement of power density of pristine and composite PCM was tested through the pressure-enhanced close contact melting (CCM) - dynPCM method (Figs. 10 and S1-S2). The PCM container for the experimental test section is made of plexiglass with cylindrical shape (inner diameter of 30 mm; height of 100 mm). Four K-type thermocouples are embedded in the base of the PCM container and measure the temperature 3 mm below the interface between PCM and container (Fig. S2). Considering the high TC of copper (398 W/m·K), temperature measurement was conducted 3 mm below the PCM and Cu plate interface, assuming to reflect the temperature progress precisely. A Peltier cell (4.0 cm × 4.0 cm) was placed at the bottom of the sample container and a DC power controller was used to supply a constant heating flux (1.9 W/cm^2). Continuous application of pressure on the solid PCM sample is developed by the piston through the mass weight applied on the top. The sample and piston diameter are kept at 20 mm, which helps to maintain adequate space for the flow of liquid PCM (melted portion). The experimental measurement for evaluating the thermal performance of pristine and dynPCM were carried out at room temperature (~25 °C), and variation of the temperature characteristics of the heat source (interface) was measured by K-type thermocouples (accuracy: ±1.5 °C) connected with the data acquisition system. Each measurement was performed thrice, and the mean value and the corresponding standard deviation were reported.

As a reference, Fig. 3(g) shows DSC curves of pristine LA: results revealed melting and solidification temperatures equal to 45.4 °C and 40.1 °C, respectively. The latent heat of pristine PCM during melting and solidification phase transition processes amounted to 172.5 and 170.4 J g^{-1}, respectively. These thermal properties of LA find good agreement with previous results in the literature [60,61].

3. Results and discussion

3.1. Composite PCMs boost heat conduction performance

Figs. 4(a) and (b) show the variations in thermal conductivity and thermal diffusivity of the PCM as a function of CBNP and GNP loading concentrations. The measured values of thermal conductivity, diffusivity, and volumetric heat capacity of LA are found in good agreement with the previous literature [62–64]. In detail, the thermal conductivity and diffusivity of PCM effectively increased from 0.219 to 0.333 W/m·K (i.e., ~50 %) and from 0.102 to 0.276 mm^2/s, respectively, as the concentration of CBNP increased to about 5 wt. %. Fig. 4(b) shows that the thermal conductivity of PCM effectively increased from 0.219 to 0.386 W/(m·K) (i.e., ~76 %) for 4 wt. % GNP loadings. However, in both cases, beyond 4–5 wt. % loading concentration, the heat conduction enhancement of composite PCM significantly decreased, which may be attributed to the formation of larger particle clusters and thus poor dispersion within the medium and possible phonon scattering as highlighted in previous studies [65–68]. Fig. 4(c) indicates that the volumetric heat capacity of the CBNP and GNP-loaded composite PCMs decreased compared to pure PCM with the loading filler concentrations, due to the lower thermal capacity of carbon fillers than the PCM one. We observed at 6 wt. % loading a decrement of volumetric heat capacity of

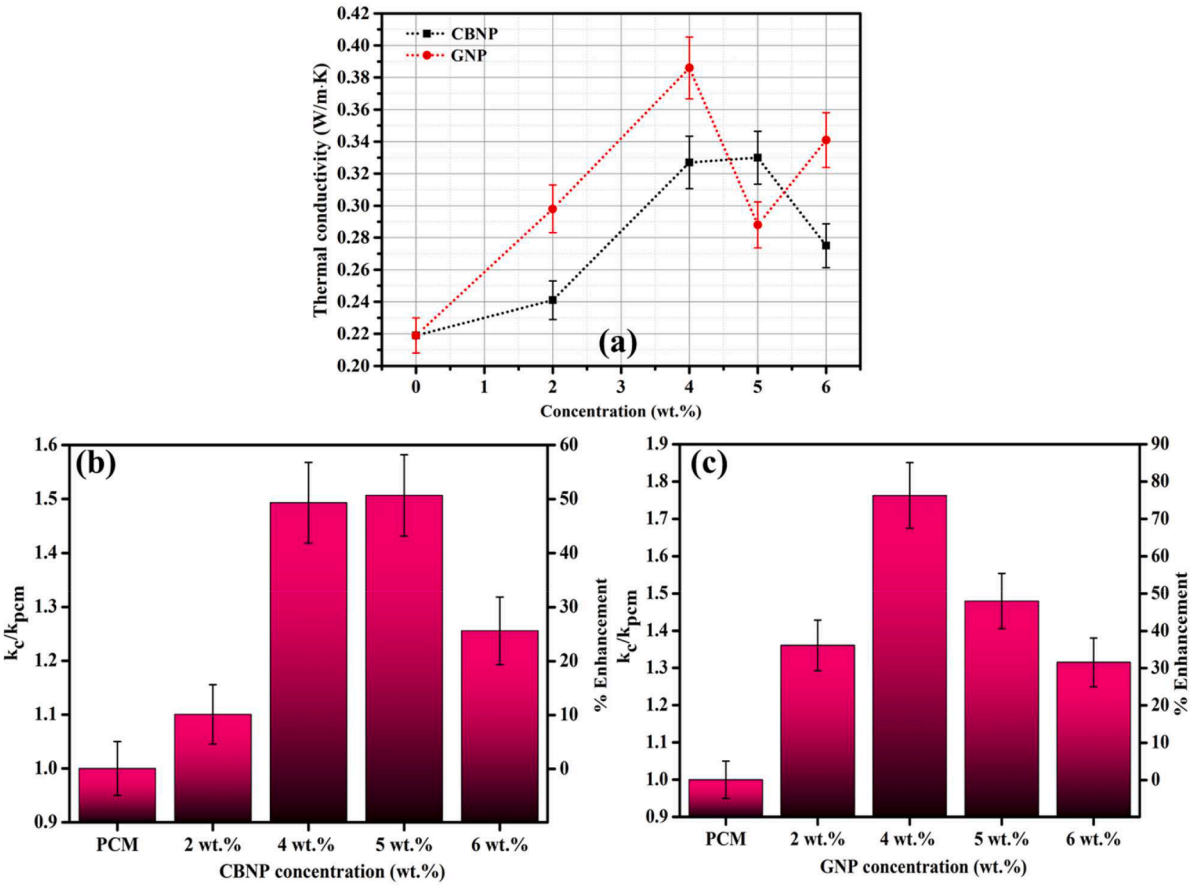

Fig. 7. (a) Variation of TC of composite PCMs loaded with various concentrations of CBNP and GNP. (b)-(c) Variation of k_c/k_{pcm} and enhancement (%) for PCM at different CBNP and GNP loadings. k_{pcm} and k_c refer to the TC of pristine PCM and composite PCM, respectively. The TC enhancement percentage in composite PCM was calculated using the expression $\left(k_c/k_{pcm} - 1\right) * 100$.

~50.5 and 52.7 % for CBNP and GNP-based composite PCM, respectively. Similarly, Wong et al. [69] reported a ~53.2 % decrease in volumetric heat capacity for 5 wt. % GO/paraffin composite PCMs with respect to the pristine one.

Figs. 5(a) and (b) show the heat flow curves, during melting, for the PCMs loaded with various concentrations of CBNP and GNP nanofillers, respectively. Figs. 5(c)-(d) show the heat flow curves, during freezing, for the same samples. The heat flow curves for constituent elements of composite PCMs viz. pristine PCM and respective incorporated pure nanofillers (CBNP/GNP) are also compared. It can be seen from Figs. 5 (a)-(d) that the heat flow curves consisted of a single endotherm (energy absorbed) or exotherm (energy released), indicating the first-order solid-liquid phase transitions. The latent heat values were determined from the areas under the heat flow curves of PCM and composite PCMs, respectively. It is evident from Table 2 that the phase transition temperatures did not vary significantly with the increasing loading of the nanofiller, which indicated the absence of any effective interactions between the filler and the target host matrix. An overview of the measured thermal properties is reported in Table 2.

Figs. 6(a)-(b) shows that increasing the loading of the nanofiller leads to a reduction in latent heat. This is attributed to the mass percentage of pristine PCM progressively decreasing in the composite with increasing nanofiller particles, which do not contribute to latent heat storage. The latent heat values were also theoretically calculated for the different composite PCM, using the formula: $\Delta H_{CPCM} = \varepsilon * \Delta H_{PCM(LA)}$ [70], where ΔH_{CPCM}, $\Delta H_{PCM\ (LA)}$ and ε indicate the calculated latent heat of the composite PCMs, the experimentally determined latent heat for pristine LA and the mass percentage of the host matrix (PCM) in the composite, respectively. The experimental findings indicated that ~8.3 % and 11.7 % decrement of latent heat occurred with the maximum loading at 6 wt. % of CBNP and GNP nanofiller in the composite PCM. Figs. 6(c)-(d) show the specific heat capacity of pristine PCM and filler-loaded composite PCMs.

The examined c_p value (~2.03 J/g·K) for LA is showing good agreement with literature data at room temperature [63]. The observed decrement of c_p of composite PCMs with the filler loading is attributed to the reduction of PCM mass content and incorporated fillers (CBNP and GNP) having poor c_p compared to the host matrix [71–73]. The experimental findings show composite PCMs (2 wt. % CBNP) (Fig. 6(c)) have a higher c_p value than pure PCM. Previously, Hu et al. and Amin et al. reported that a low concentration of nanofillers, such as SiO_2 and GNP, improved the specific heat capacity of the medium because of variation in coulombic energy due to clustering and changes of interaction behaviour among nanoparticles, which helped to increase the surface energy and boosted heat capacity [74,75].

Fig. 7(a) shows the variation of TC of composite PCMs as a function of the loading concentration of the CBNP and GNP fillers. Our results show that the TC does not linearly increase with filler loadings in composite PCM. Fig. 7(b) shows that the thermal conductivity of CBNP-loaded composite PCMs increased significantly (~50 %) as the CBNP loading rose from 2 to 5 wt. %. In comparison, GNP-based composite PCMs (see Fig. 7(c)) achieved a higher enhancement (~76 %) with a GNP loading range of 2 to 4 wt. %. The better TC enhancement of GNP-loaded composite PCMs respect to CBNP one could be attributed to 2D structure of GNPs, which typically has the ability to comparatively build better percolation pathways [64,76]. As a matter of fact, Yang et al. [77], using molecular dynamics simulations, demonstrated that GNPs act as nucleation sites during solidification, inducing orientational

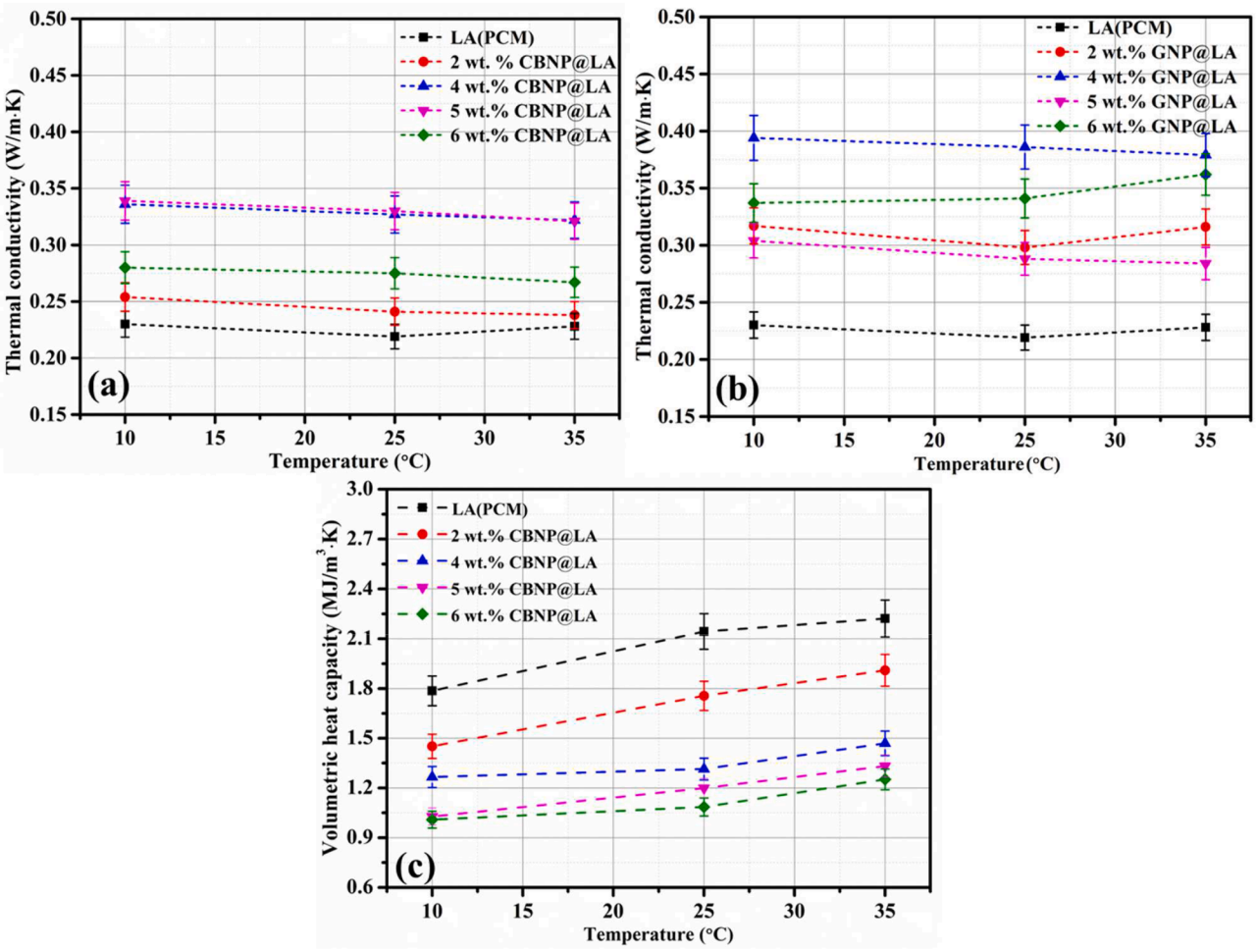

Fig. 8. Variation of thermal conductivity, as a function of temperature for nanofiller loaded composite PCMs at their different concentrations: (a) CBNP; (b) GNP. (c) Variation of volumetric heat capacity of CBNP-loaded composite PCM as a function of temperature. For comparison, variation of TC and volumetric heat capacity of pristine PCM is also shown in the figures.

ordering at the GNP-PCM interface and enhancing phonon coupling.

Similarly, studies by Fan et al. [71] and Zakaria et al. [78] highlighted GNP's superiority in TC enhancement compared to other nanofillers (e.g., multi-walled carbon nanotubes), owing to its high surface area, planar structure (enabling plane-to-plane contact), and reduced interfacial thermal resistance. Despite the lower bulk thermal conductivity of CBNP (~0.25–4.0 W/m·K) relative to GNP (~3000 W/m·K) [79], its significant TC enhancement (~50 %) is attributed to its high compressibility, excellent volume-filling capability, and the fractal nature of its aggregates. The low fractal dimension of CBNP aggregates promotes the formation of percolating networks with improved interfacial interactions between aggregates and PCM, reducing phonon scattering and Kapitza resistance [16,30]. This clearly showed that effective TC enhancements of composite PCMs are influenced by various factors viz. bulk thermal conductivity of filler, aggregation dynamics, fractal structures, Kaptiza resistance, and segregation characteristics [68,64,80]. At higher loadings, the observed heat transfer efficiency is reduced due to the domination of effective particle clustering and settling issues. As found, GNP enhanced the TC of composite PCMs more effectively compared to CBNP. However, while GNP provides superior TC enhancement, CBNP's significantly lower cost (10 times less than GNP) makes it a more economically viable option for widespread applications.

Figs. 8(a)-(b) show the variation of thermal conductivity of CBNP and GNP loaded composite PCMs (solid state) at various loadings as function of temperature. Results show that the thermal conductivity of PCM and its composites does not effectively change with the temperature variation. Similarly, Fang et al. [81] and Warzoha et al. [82] reported that the thermal conductivity of PCM and related composites are almost independent of temperature in their solid and liquid phase. This can be attributed to the stable phonon heat conduction capability and consistent microstructural stability across the measured temperature range. Similarly, Fig. 8(c) shows the variation of volumetric heat capacity of different CBNP-loaded composite PCMs as function of temperature, highlighting a moderate impact of temperature, coherently with previous studies [81].

The assessment of repeatable (thermal stability) thermal response (after several phase change cycles) of nanocomposite PCMs is essential for practical TES applications in the long term. To probe the composite PCMs' thermal stability in comparison to pristine PCMs, DSC studies were carried out over 100 successive thermal cycles with and without filler loading. It can be seen from Figs. 9 (a)-(b) that the heat flow characteristics (phase transition temperature and latent heat value) of pristine PCM and their respective (4 wt. %) loaded CBNP and GNP composite PCM were almost unchanged. The measured latent heat values of pristine PCM and (4 wt. %) CBNP/GNP composite PCMs were ~ 170.2, ~ 158.5, and ~ 156.3 J/g, respectively, even after 100 cycles (reduced ~ 3 %), which indicates their practical potential for TES systems. Furthermore, the durability of the heat conduction performance of respective nanocomposite PCMs was also analyzed after prolonged 1st, 5th, and 10th phase change cycles (Fig. 9(c)). The TC results attributed that repeated melting/solidification process effectively induced particle

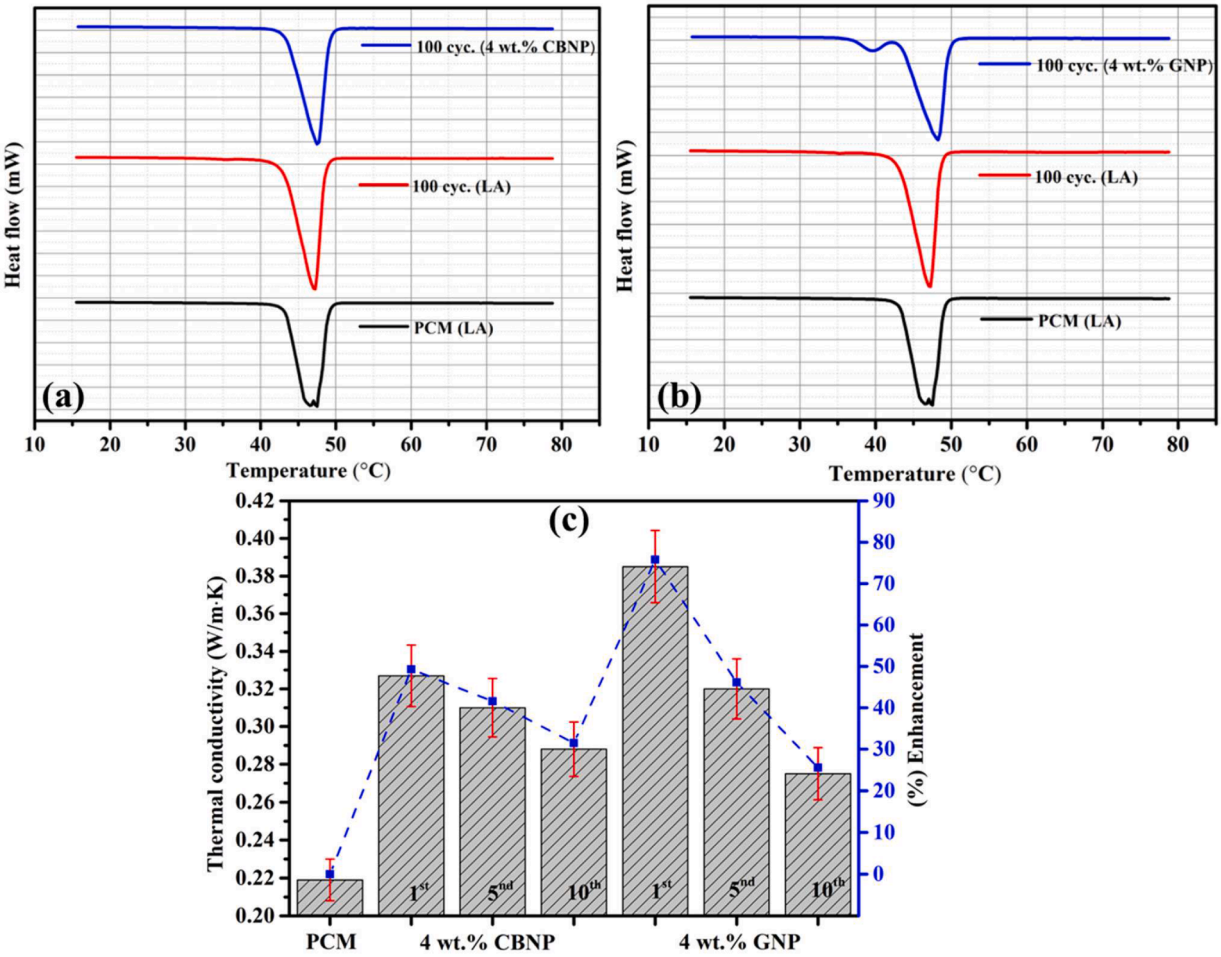

Fig. 9. (a)-(b) Heat flow curves after 100 thermal cycles of pristine PCM (LA) and 4 wt. % loaded CBNP and GNP composite PCMs. (c) durability of heat conduction performance after the 1st, 5th and 10th thermal cycles, respectively. Thermal characteristics of pristine PCM are also shown for comparison.

agglomeration inside the PCM matrix and created bigger-sized clusters (prone to settle down) due to the action of gravity. Therefore, the dispersion volume of effective heat carriers (percolation pathways) goes down in the medium and hampers the heat conduction capacity.

3.2. *Composite PCMs boost thermal management performance*

Fig. 10(a) shows a schematic illustration of constrained melting, gravity-driven CCM, and pressure-enhanced CCM (dynPCM). For constrained melting and gravity-driven melting cases, the melt front thickness (δ) increases quickly, and it continuously grows over time (denoted by red arrows) thus reducing the power density of TES system. However, δ can be effectively minimized (thin melt-front maintained over the entire melting process) by the dynPCM approach, with a boost in the heat transfer rate during the melting phase. To quantify this effect, the performance of both pristine and nano-enhanced composite PCMs was evaluated during the melting process using the dynPCM approach. A constant heat flux (q" = 1.9 W cm^{-2}) was supplied using a Peltier cell, while stable pressure was maintained by placing a 2 kg mass on top of a piston. The detailed working mechanism of the designed prototype dynPCM setup is illustrated in Figs. S1-S2.

Experimental data from Fig. 10(b) highlights the variation in heat source interface temperature (T_s) under dynPCM, showcasing distinct thermal characteristics compared to copper plates (without PCM), constrained melting, and gravity-driven melting. DynPCM achieved stable temperature control and minimized the superheat degree by approximately 10 °C until complete melting. This demonstrates that the dynPCM method enables spatial control of the melt front location by accelerating the discharge flow of superheated liquid PCM, significantly reducing melt layer thickness and interface thermal resistance and improving power density compared to conventional melting strategies. Fig. 10(c) illustrates the T_s variation for PCM and CBNP-loaded composite PCMs under the dynPCM scheme. The inset provides a magnified view of T_s as a function of time, showing that the 2 wt. % CBNP composite PCM may improve power density. The reduction in power density at higher CBNP loadings might be attributed to a viscosity increase (~70 %, Fig. 11), although further investigations are still needed in this respect.

We expect that an enhanced viscosity may hinder the discharge flow of superheated liquid PCM, reducing convective heat transfer and power density. Similarly, Li et al. [58] observed that the nanofiller-induced viscosity increment negatively impacts power density and TES performance of composite PCMs. The enhanced performance of 2 wt. % CBNP loading is attributed to its optimal balance between heat transport capability and viscosity, which remains close to that of the pristine PCM, making it a more effective candidate for thermal management applications. These findings demonstrate that the designed dynPCM setup (the presence of forced convection and not only natural convection/standard static configurations holds the potential to greatly alleviate the issues of particle sedimentation and composite stability) is capable of significantly improving heat storage and enabling high-performance thermal management applications.

Fig. 11 shows the variation of dynamic viscosity of liquid PCM at 55 °C as a function of nanofiller loadings. Results show that the dynamic

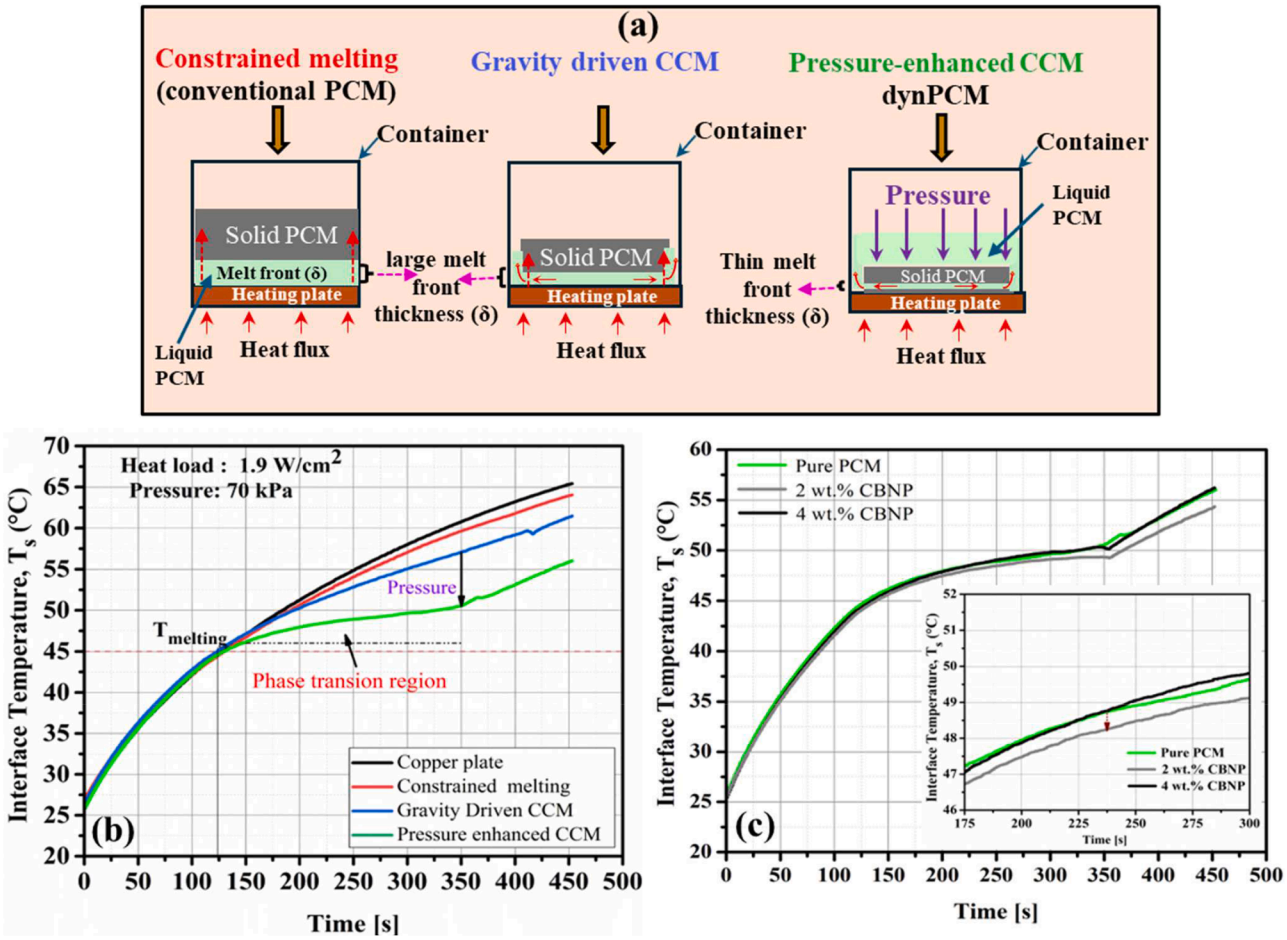

Fig. 10. (a) Schematic illustration of different PCM melting approaches. (b)-(c) Thermal management performance of PCM and composite PCM under dynPCM scheme, respectively.

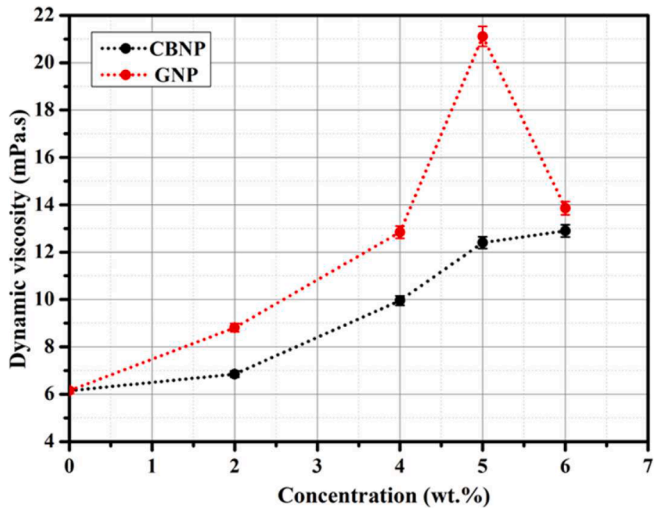

Fig. 11. Variation of dynamic viscosity of composite PCM as a function of CBNP and GNP loadings.

viscosity of liquid PCM effectively increases with CBNP and GNP concentration. The dynamic viscosity of LA at 55 °C shows good agreement with data reported by Anggraini et al. [83]. The rate of dynamic viscosity increase for CBNP composite PCM decreases at higher loadings, while for GNP composite PCM, viscosity effectively decreases due to the formation of larger aggregates that are prone to sedimentation. These viscosity measurements provide valuable insights into the reduction of TC enhancement at high filler loadings, attributed to the development of larger aggregates (Figs. 4 and 7). Notably, a significant increase in the viscosity of liquid PCM negatively impacts heat transport efficiency by suppressing natural convection driven by buoyancy effects, which in turn reduces the power density during the charging (melting) process [22,10,84]. Similarly, Kittusamy et al. [85] and Cabaleiro et al. [86] reported that incorporating 3 wt. % GNP and 1 wt. % CBNP significantly increased the viscosity of liquid PCM. Therefore, optimizing the nanofiller loading ratio in composite PCMs is crucial to achieving the best performance among different nanofillers.

3.3. Composite PCMs boost photothermal and solar-thermal-electric conversion performance

Fig. 12(a) reports a schematic diagram of the photothermal conversion performance investigation. The photothermal conversion and storage properties of PCM and nanofillers (CBNP and GNP) loaded composite PCM were evaluated under simulated sunlight irradiation at an intensity of 150 mW/cm^2. Fig. 12(b)-(c) displays the temperature variation curves of different samples, which were recorded by a data acquisition system (time−temperature data recorded using a thermocouple recorder connected to the computer). Solar irradiation causes the temperature of composite PCMs to rise sharply, contrary to the case of pure PCMs. Moreover, in the phase transition zone, the temperature stabilizes on a plateau value. In this region, PCM starts to change from solid to liquid. This process will absorb part of the heat (gained from the

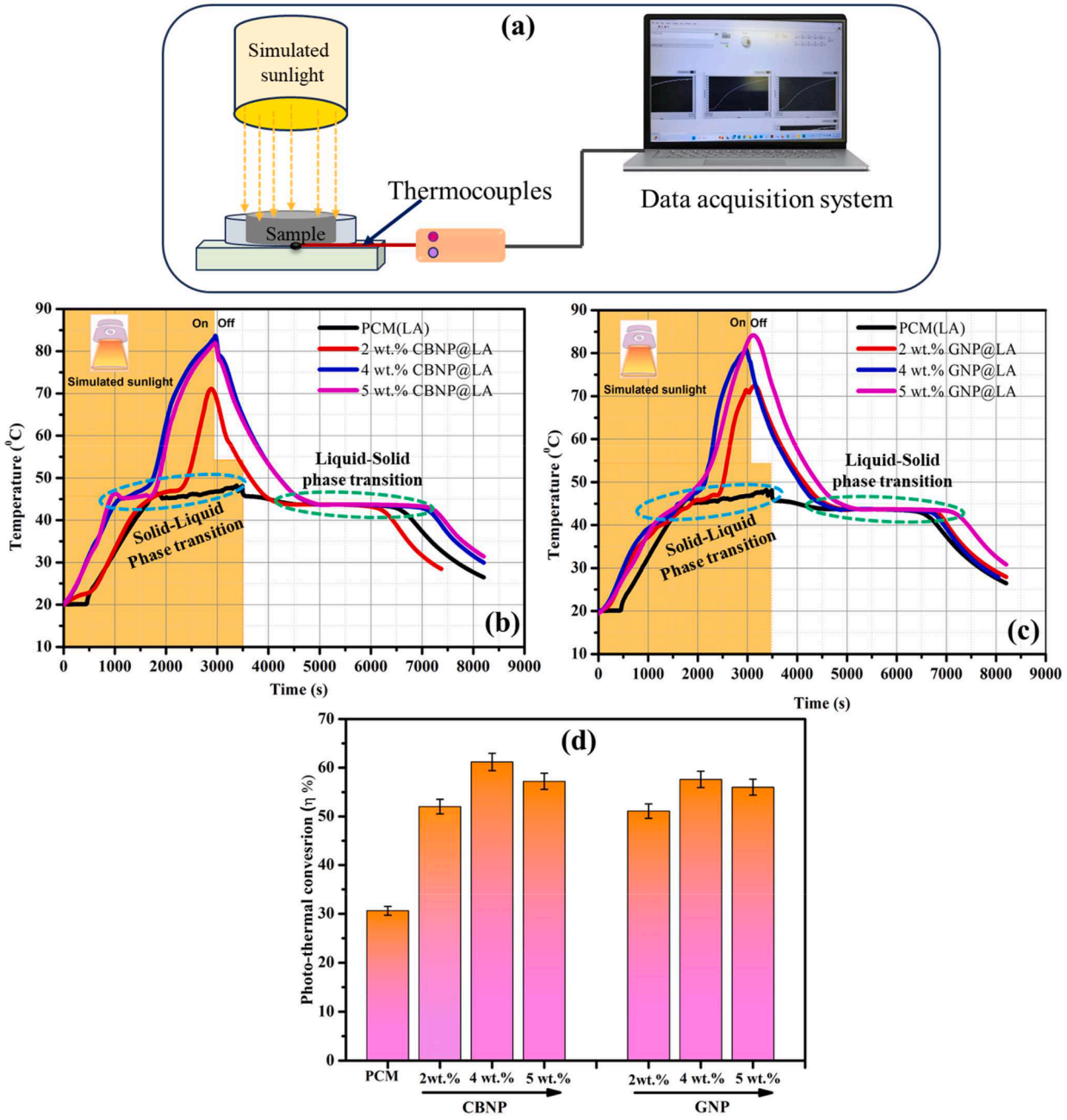

Fig. 12. **(a)** Schematic representation of photo-thermal measurement setup; (b)-(c) photothermal conversion for pristine PCM and CBNP and GNP-based composite PCMs at various loadings. (d) Variation of photothermal conversion efficiency as a function of concentrations.

photothermal process), thereby the temperature rise will slow down, which causes a slower temperature rise due to high latent heat values. When light irradiation was turned off, the temperature drop happened sharply, and further, when the temperature reached the crystalizing point another plateau appeared (the stored latent heat is released during the cooling process). Experimental results indicate that CBNP and GNP nano-additives significantly improved the photothermal conversion performance of PCM. These carbon-based nanofillers act as strong photon absorbers and molecular heaters to transform light into heat energy within PCM.

Wang et al. [87] and Du et al. [35] demonstrated that carbon-based nano-additives (CNTs) have a remarkable capability to absorb ultraviolet and visible light compared with pristine PCM, and show resonant π-plasmon excitation and band-to-band transitions under solar radiation. He et al. [33] and Elbasiony et al. [88] reported that GNP has zero bandgap structure characteristics, enhancing solar light absorption by surface plasmon resonance or intensive scattering. Fan et al. [45], Mishra et al. [16,30], Zhang et al. [70] and Han et al. [89] have demonstrated that CBNP nanofiller has high solar light absorption capability and effectively helps to boost the PTC performance of the pristine PCM and aqueous medium with an augmentation of the extinction coefficient of the incident light due to multiple scattering and trapping of photons. The temperature rise was not linearly increased with filler loading amount into the host matrix, however beyond a certain loading of CBNP and GNP the photothermal conversion performance begins to decline (Fig. 12(d)). Yang et al. [44] reported that as the nanofiller concentration increases, the ratio of surface reflection and nanoparticle aggregation within the medium becomes more pronounced and affects the PTC activity. The presence of larger filler aggregates or cluster structures interferes significantly with the transparency of the

Table 3
Photothermal conversion-related parameters of samples.

Sample	Mass (g)	*Phase change interval* (t_e - t_s) sec	Latent heat (J/g)	Area (cm^2)	Light intensity (mW/cm^2)	η (%)
PCM (LA)	32	1690	172.5	71	150	30.6
2 wt. % CBNP	32	985	170.5	71	150	52.0
4 wt. % CBNP	32	800	163.2	71	150	61.2
5 wt. % CBNP	32	870	160.1	71	150	57.2
2 wt. % GNP	32	982	168.5	71	150	51.1
4 wt. % GNP	32	873	163.2	71	150	57.6
5 wt. % GNP	32	840	157.1	71	150	56.0

Table 4
Comparison of TC enhancement and photothermal efficiency with previous works.

Sample (composite PCMs)	Filler Concentration	TC enhancement (%)	Photothermal efficiency (%)	Ref.
LA + graphene (Gr)	0.7 wt %	18.4	–	[97]
LA + graphene aerogel + RGO	5 wt %	288.4	79.5	[98]
LA-SA + silicon carbide (SiC)	0.075 Vol %	75.8		[99]
LA+ expanded graphite (EG)	5 wt %	750	62	[91]
LA-SA + copper oxide (CuO)	0.2 wt %	30.0	–	[100]
LA+ silver (Ag) + Graphene (Gr)	4 wt %	55	–	[101]
LA+ expanded perlite + EG	10 wt %	86	–	[102]
LA + SWCNT	2 Vol %	37		[103]
Paraffin wax +Ti_2O_3	9 wt %	37.8	76.96	[104]
Paraffin + EG +CB	10 wt %	–	60.1	[105]
Paraffin + POE +EG	7 wt %	127	58.2	[106]
LA + *h*-BN	2 wt %	27		[107]
LA+CBNP, LA+GNP	**4 wt %**	**~ 50, ~76**	**~ 60.1, ~ 57.6**	**Present study**

glass, causing excessive scattering and reflection of light. As a result, the ability to effectively capture sunlight energy is reduced.

The photo-thermal conversion efficiency (η) is defined as the ratio of the thermal energy stored during the phase change process to the incident light energy, calculated by the following Eq. (1) [90,91],

$$\eta = \frac{m_s * \Delta H_s}{I * A(t_e - t_s)} \quad (1)$$

where m_s, ΔH_s, I and (t_e - t_s) indicate the mass of the specimen, latent heat, the illumination intensity (simulated sunlight), specimen area that receives light and phase change interval (t_e and t_s indicating phase transition ends and starts time), respectively. The photothermal conversion efficiency (η) of pure PCM and their different CBNP and GNP loading were calculated. The η (%) values of pure PCM, 2 wt. %, 4 wt. % and 5 wt. % CBNP loaded composite PCMs are 30.6 %, 52.0 %, 61.2 % and 57.2 %, respectively. The case of GNP loaded 2, 4, and 5 wt. % achieved 51.1 %, 57.6 % and 56 %, respectively. This achieved high PTC efficiency with CBNP and GNP nanofillers is justified by their excellent light absorption characteristics in the UV–Vis-NIR region and potential for solar-thermal applications.

The above experimental results (Table 3) show the PTC performance of CBNP-based composite PCM is better compared to GNP-based composite PCM. This could be attributed to CBNP having better broad-spectrum light absorption compared to GNP [79,92]. Found apart from nanofiller loading concentration, solar illuminating intensity also effectively effects PTC performance [93,94]. Yang et al. [91] reported η is 62 % for 5 wt. % EG/LA at 100 mW/cm^2. Furthermore, the optical properties and PTC performance of carbon-based fillers strongly depend upon their morphological characteristics viz. shape, size, number of layers and doping [95,96]. The PTC study-related parameters are listed in Table 3.

Table 4 compares the TC enhancement and photothermal conversion efficiency of the current findings to other organic PCM-based nano-enhanced composite PCMs. It can be noticed the prepared lauric acid (LA) based nanocomposite PCMs (utilized cost-effective carbon-based nanofillers for direct mixing) are very economical and significantly improved heat conduction and photothermal characteristics.

Fig. 13(a) shows a schematic illustration of solar-thermal-electric energy conversion in the presence of composite PCM and Fig. 13(b) shows the output voltage evolution curves in the presence of PCM and composite PCMs under light irradiation (150 mW/cm^2). These samples were chosen as heat sources for the solar thermoelectric generator. The PCM-based sample was exposed to the simulated solar irradiation and fixed on the hot end of a commercially available thermoelectric conversion module (5.5cm × 5.5 cm) and, the cold end of the module (maintained ~21 °C) was attached to an aluminium based heat sink. During the operation, a digital voltage meter measured the open-circuit voltage of the thermoelectric module. It can be seen the performance (output) increases with sunlight exposure time due to the effective conversion of absorbed sunlight into thermal energy. It is worth noting that near the phase transition region the yield is stable, while an effective increase occurs after the melting process is completed. It is worth noticing that solar thermoelectric performance of CBNP and GNP-based composite PCMs is better than pristine PCMs, achieving a maximum of ~ 23 % and ~ 36 % enhancements, respectively. This is attributed to CBNP and GNP composite PCMs containing high light-heat conversion capacity (PTC efficiency) and better heat transport characteristics.

Such kind of carbon-based nanofillers have strong UV–Vis-NIR light absorption ability [108,109,45] that help to boost solar-thermal-electric conversion. The maximum achieved output is ~600, 730 and 815 mV for PCM, 4 wt. % CBNP and GNP loaded composite PCM, respectively. GNP-loaded composite PCM shows superior performance compared to other samples, which could be due to the synergic meeting of improved PTC and quick heat deposit ability to the thermoelectric module. When the light source is removed the output decreases (stop photothermal-conversion) and natural cooling starts, again stable output appears across solidification temperature due to the release of stored latent heat that provides heat to TEG until the completion of solidification. The solar-thermal-electric conversion significantly depends upon the intensity of irradiated solar light [110].

In previous studies, Usman et al. [28] for MXene-Integrated composite PCM achieved 750 mV (~ 125 mW cm^{-2}), Hu et al. [111] found ~409 mV for MH-AlN/SA (~74 mW cm^{-2}) and Chen et al. [90]

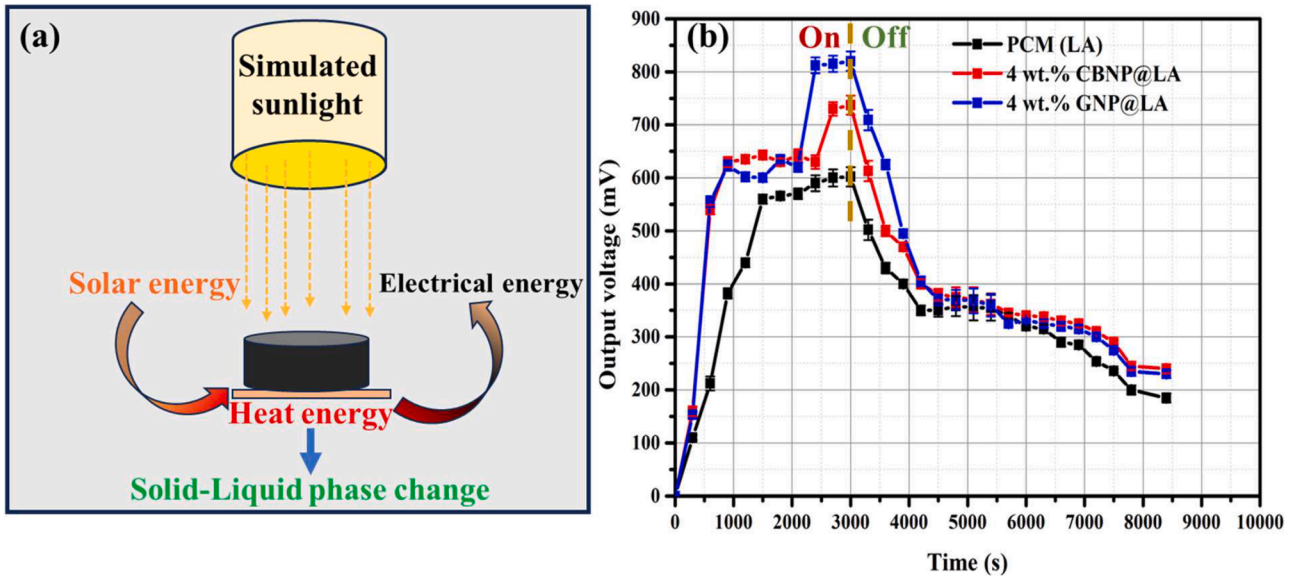

Fig. 13. (a) Schematic illustration of Solar-Thermal-Electric energy conversion. (b) Output voltage evolution curves of PCM and composite PCMs as a function of light irradiation exposer.

Table 5
Comparison of TEG output performance with previous works.

Sample type	Concentration	TEG output (mV)	Ref.
M-SSPCMs	5 wt. % $Ti_3C_2T_x$	750	[28]
MH-AlN/SA	44.46 vol % AlN	409	[111]
PW/CRGO15–30 %	30 % CNT	150	[90]
CBNP@LA, GNP@LA	**4 wt. % CBNP/GNP**	**730, 815**	**Present study**

observed ~150 mV (100 mW cm^{-2}) for PW/CRGO composite PCM under solar irradiation, respectively. These experimental results confirm that incorporating CBNP and GNP nanofillers holds significant potential for enhancing the photothermal conversion efficiency and solar thermoelectric performance of pristine PCM. Table 5 summarizes the current TEG findings with previously reported TEG results.

4. Conclusion

In this work, significant enhancements in thermal energy storage and management performance of pristine PCM were achieved through the integration of dynamic PCM and nanofiller characteristics. In particular, ~76 % thermal conductivity improvement and ~ 61 % photothermal conversion efficiency with 4 wt. % loading of GNP & CBNP-based composite PCM have been achieved, respectively, and this is because these nanofillers provide superior heat conducting pathways and have strong light absorption characteristics.

We demonstrated that the dynamic PCM (dynPCM) strategy improves power density and heat storage characteristics (charging process), and it exhibits superior potential to overcome the limitations of poor thermal conductivity and stability challenges in pristine/nano-enhanced PCM cases, respectively, for long-term use in TES applications. Our experimental findings comprehensively explore (in much detail for the first time) the importance of nanofillers' characteristics (physical, morphological, and loading ratio) on the various thermophysical and optical characteristics (i.e. heat conduction, latent heat, volumetric heat storage capacity, viscosity, photothermal, and solar-thermal-electric performances) of the composite PCMs.

The heat conduction, effective thermal energy storage, and photothermal conversion performance were reported for lauric acid (LA)-based composite PCM loaded with various concentrations of CBNP and GNP. DSC findings indicated that phase change characteristics of composite PCMs remained almost constant, while latent heat storage ability slightly decreased with filler concentrations, whereas nanoparticle loadings effectively influenced the thermophysical properties of composite PCMs, and high viscosity hampered the convective heat transfer and photothermal conversion rate during the melting process.

Our designed pressure-enhanced CCM (dynPCM) setup creates a very thin melt layer, which helps minimize thermal resistance (melt front thickness at the interface) and boosts the thermal management performance of the PCM for the high heat flux of electronic devices. The dynPCM findings show that the optimum loading of the nanofiller further enhanced the thermal response (power density) due to synergistically showing a better heat flow (conduction) and a minimal impact on melt-front dynamics. In the present report, we explore the importance of thermophysical properties, pressure-enhanced CCM, and optical characteristics of carbon-based composite PCMs towards advancing latent thermal energy storage and management strategy compared to conventional pristine PCM-based techniques.

Funding information

We acknowledge the financial support of the research contract PTR 2022/24 - ENEA (Studio di sistemi di accumulo termico innovativi basati sull'utilizzo di nano-PCM dinamici: Modellazione e analisi sperimentale delle proprietà termofisiche, realizzazione e testing di un prototipo, e analisi delle possibili applicazioni di tale tecnologia nell'ambito dell'accumulo termico) funded by Ministero dell'Ambiente e della Sicurezza Energetica (MASE).

CRediT authorship contribution statement

Amit Kumar Mishra: Writing – review & editing, Writing – original draft, Visualization, Validation, Methodology, Investigation, Formal analysis, Conceptualization. **Matteo Morciano:** Writing – review & editing, Methodology, Investigation, Data curation. **Biruk Wondifraw Agegnehu:** Writing – review & editing, Visualization, Investigation, Data curation. **Elena Campagnoli:** Writing – review & editing, Methodology, Investigation, Data curation. **Valter Giaretto:** Writing – review & editing, Methodology, Investigation, Data curation. **Andrea Bottega:** Writing – review & editing, Methodology, Investigation. **Matteo**

Fasano: Writing – review & editing, Supervision, Methodology, Formal analysis, Data curation. **Luigi Mongibello:** Writing – review & editing, Supervision, Methodology, Investigation, Formal analysis. **Eliodoro Chiavazzo:** Writing – review & editing, Supervision, Resources, Project administration, Funding acquisition, Conceptualization.

Declaration of competing interest

The authors declare the following financial interests/personal relationships which may be considered as potential competing interests:

Eliodoro Chiavazzo reports was provided by Ministero dell'Ambiente e della Sicurezza Energetica (MASE). If there are other authors, they declare that they have no known competing financial interests or personal relationships that could have appeared to influence the work reported in this paper.

Acknowledgments

We are grateful to Luca Lavagna and Alessio Modello for helping with the FESEM measurements.

Supplementary materials

Supplementary material associated with this article can be found, in the online version, at doi:10.1016/j.ceja.2025.100789.

Data availability

Data will be made available on request.

References

[1] Z. Zhao, et al., Carbon-based phase change composites with directional high thermal conductivity for interface thermal management, Chem. Eng. J. 496 (July) (2024), https://doi.org/10.1016/j.cej.2024.154305.
[2] W. Chu, N. Duić, Q. Wang, Recent advances in energy storage and energy saving technologies: SDEWES special issue in 2022, Energy Storage Sav. 3 (1) (2024) 1–4, https://doi.org/10.1016/j.enss.2023.09.001.
[3] J. Li, et al., Recent advances and perspectives in solar photothermal conversion and storage systems: a review, Adv. Colloid. Interface Sci. 325 (2024) 103118, https://doi.org/10.1016/j.cis.2024.103118.
[4] W. Lin, J. Lai, K. Xie, D. Liu, K. Wu, Q. Fu, D-mannitol/graphene phase-change composites with structured conformation and thermal pathways allow durable solar-thermal-electric conversion and electricity output, ACS. Appl. Mater. Interfaces. 14 (34) (2022) 38981–38989, https://doi.org/10.1021/acsami.2c11843.
[5] D. Liu, C. Lei, K. Wu, Q. Fu, A multidirectionally thermoconductive phase change material enables high and durable electricity via real-environment solar-thermal-electric conversion, ACS. Nano 14 (11) (2020) 15738–15747, https://doi.org/10.1021/acsnano.0c06680.
[6] T. Boldoo, V. Chinnasamy, H. Cho, Enhancing efficiency and sustainability: utilizing high energy density paraffin-based various PCM emulsions for low-medium temperature applications, Energy (2024) 131988.
[7] R. Fan, M. Wan, T. Zhou, N. Zheng, Z. Sun, Graphene-enhanced phase change material systems: minimizing optical and thermal losses for solar thermal applications, Energy 289 (2024) 129979.
[8] V. Chinnasamy, J. Heo, S. Jung, H. Lee, H. Cho, Shape stabilized phase change materials based on different support structures for thermal energy storage applications–A review, Energy 262 (2023) 125463.
[9] S. Wang, et al., Regulating cold energy from the universe by bifunctional phase change materials for sustainable cooling, Adv. Energy Mater. (2024) 2402667.
[10] Z.R. Li, N. Hu, L.W. Fan, Nanocomposite phase change materials for high-performance thermal energy storage: a critical review, Energy Storage Mater. 55 (2023) 727–753, https://doi.org/10.1016/j.ensm.2022.12.037. August 2022.
[11] S. Zhao, et al., Elevating the photothermal conversion efficiency of phase-change materials simultaneously toward solar energy storage, self-healing, and recyclability, ACS Appl. Mater. Interfaces 14 (25) (2022) 29213–29222.
[12] H. Wang, X. Li, B. Luo, K. Wei, and G. Zeng, "The MXene /water nano fl uids with high stability and photo-thermal conversion for direct absorption solar collectors : a comparative study," vol. 227, 2021.
[13] R.A. Lawag, H.M. Ali, Phase change materials for thermal management and energy storage: a review, J. Energy Storage 55 (2022) 105602.
[14] J. He, W. Chu, Q. Wang, Experimental study on pressure-enhanced close contact melting with PCMs for stable temperature control of high heat flux electronic devices, Appl. Therm. Eng. 230 (2023) 120707, https://doi.org/10.1016/j.applthermaleng.2023.120707. PA.
[15] M. Gür, E. Gürgenç, H. Co\csanay, H.F. Öztop, Novel nano-Y2O3/myristic acid nanocomposite PCM for cooling performances of electronic device with various fin designs, J. Energy Storage 100 (2024) 113646.
[16] A.K. Mishra, B.B. Lahiri, J. Philip, Carbon black nano particle loaded lauric acid-based form-stable phase change material with enhanced thermal conductivity and photo-thermal conversion for thermal energy storage, Energy 191 (2020) 116572, https://doi.org/10.1016/j.energy.2019.116572.
[17] S. Xu et al., "Sunlight-triggered phase change energy storage composite materials for human body thermal management," 2022, doi: 10.1021/acsapm.2c01287.
[18] A. Ribezzo, G. Falciani, L. Bergamasco, M. Fasano, E. Chiavazzo, An overview on the use of additives and preparation procedure in phase change materials for thermal energy storage with a focus on long term applications, J. Energy Storage 53 (January) (2022) 105140, https://doi.org/10.1016/j.est.2022.105140.
[19] M. Gür, H.F. Öztop, F. Selimefendigil, Analysis of solar underfloor heating system assisted with nano enhanced phase change material for nearly zero energy buildings approach, Renew. Energy 218 (2023) 119265.
[20] T.B. Freeman, et al., Advanced materials and additive manufacturing for phase change thermal energy storage and management: a review, Adv. Energy Mater. 13 (24) (2023) 2204208.
[21] K. Liang, L. Shi, J. Zhang, J. Cheng, X. Wang, Fabrication of shape-stable composite phase change materials based on lauric acid and graphene/graphene oxide complex aerogels for enhancement of thermal energy storage and electrical conduction, Thermochim. Acta 664 (March) (2018) 1–15, https://doi.org/10.1016/j.tca.2018.04.002.
[22] Z. Said, et al., Nano-enhanced phase change materials: fundamentals and applications, Prog. Energy Combust. Sci. 104 (2024) 101162.
[23] S.A. Ali, et al., Advancements in thermal energy storage: a review of material innovations and strategic approaches for phase change materials, Energy Fuels (2024) 19336–19392, https://doi.org/10.1021/acs.energyfuels.4c03634.
[24] R. Wen, S. Zhu, M. Wu, W. Chen, Design and preparation of Ag modified expanded graphite based composite phase change materials with enhanced thermal conductivity and light-to-thermal properties, J. Energy Storage 41 (2021) 102936.
[25] B.M. Tripathi, S.K. Shukla, P.K.S. Rathore, A comprehensive review on solar to thermal energy conversion and storage using phase change materials, J. Energy Storage 72 (2023) 108280.
[26] M. Morciano, et al., 3D printed lattice metal structures for enhanced heat transfer in latent heat storage systems, J. Energy Storage 65 (2023) 107350, https://doi.org/10.1016/j.est.2023.107350. September 2022.
[27] A. Ribezzo, et al., Enhancement of heat transfer through the incorporation of copper metal wool in latent heat thermal energy storage systems, Renew. Energy 231 (2024) 120888.
[28] A. Usman, et al., MXene-Integrated Solid-Solid Phase Change Composites for Accelerating Solar-Thermal Energy Storage and Electric Conversion, Small. Methods (2024) 2301458.
[29] A. Aziz, et al., Contemporary nano enhanced phase change materials: classification and applications in thermal energy management systems, J. Energy Storage 75 (2024) 109579.
[30] A.K. Mishra, B.B. Lahiri, J. Philip, Superior thermal conductivity and photo-thermal conversion efficiency of carbon black loaded organic phase change material, J. Mol. Liq. 285 (2019) 640–657, https://doi.org/10.1016/j.molliq.2019.04.132.
[31] H.F. Öztop, E. Gürgenç, M. Gür, Thermophysical properties and enhancement behavior of novel B4C-nanoadditive RT35HC nanocomposite phase change materials: structural, morphological, thermal energy storage and thermal stability, Sol. Energy Mater. Sol. Cells 272 (2024) 112909.
[32] A. Ribezzo, L. Bergamasco, M. Morciano, M. Fasano, L. Mongibello, E. Chiavazzo, Experimental analysis of carbon-based Phase Change Materials composites for a fast numerical design of cold energy storage systems, Appl. Therm. Eng. 231 (July 2022) (2023) 120907, https://doi.org/10.1016/j.applthermaleng.2023.120907.
[33] L. He, H. Wang, H. Zhu, Y. Gu, X. Li, X. Mao, Thermal properties of PEG/graphene nanoplatelets (GNPs) composite phase change materials with enhanced thermal conductivity and photo-thermal performance, Appl. Sci. 8 (12) (2018) 2613.
[34] S. Wu, et al., Dual-functional aligned and interconnected graphite nanoplatelet networks for accelerating solar thermal energy harvesting and storage within phase change materials, ACS Appl. Mater. Interfaces 13 (16) (2021) 19200–19210.
[35] X. Du, J. Xu, S. Deng, Z. Du, X. Cheng, H. Wang, Amino-Functionalized Single-Walled Carbon Nanotubes-Integrated Polyurethane Phase Change Composites with Superior Photothermal Conversion Efficiency and Thermal Conductivity, ACS. Sustain. Chem. Eng. 7 (21) (2019) 17682–17690, https://doi.org/10.1021/acssuschemeng.9b03853.
[36] W. Luo, et al., Highly thermal conductive phase change materials enabled by CNTs-modified PVA aerogel for solar energy storage and thermal management of electronic components, J. Energy Storage 88 (2024) 111583.
[37] W. Wang, et al., Ultralight and flexible carbon foam-based phase change composites with high latent-heat capacity and photothermal conversion capability, ACS Appl. Mater. Interfaces 11 (35) (2019) 31997–32007.
[38] Y. Huo, T. Yan, X. Chang, W. Pan, Expanded graphite@ octadecanol composite phase change material with photothermal conversion interface, Sol. Energy 263 (2023) 111922.
[39] Y. Deng, J. Li, H. Nian, Polyethylene glycol-enwrapped silicon carbide nanowires network/expanded vermiculite composite phase change materials: form-stabilization, thermal energy storage behavior and thermal conductivity enhancement, Sol. Energy Mater. Sol. Cells 174 (2018) 283–291, https://doi.org/10.1016/j.solmat.2017.09.013. June 2017.

[40] M. Gür, E. Gürgenç, H. Co\csanay, H.F. Öztop, Solar-assisted radiant heating system with nano-B4C enhanced PCM for nearly zero energy buildings, Case Stud. Therm. Eng. 65 (2025) 105544.
[41] J. Qiu, M. Xie, T. Wu, D. Qin, Y. Xia, Gold nanocages for effective photothermal conversion and related applications, Chem. Sci. 11 (48) (2020) 12955–12973.
[42] M. Du, et al., CuS nanoparticle-based microcapsules for solar-induced phase-change energy storage, ACS. Appl. Nano Mater. 5 (9) (2022) 13009–13017.
[43] B. Zhao, R. Zhu, N. Sheng, C. Zhu, Z. Rao, Composite phase change material supported by cu nanoparticles@ carbon porous matrix for photo-thermal energy storage, Energy Fuels 36 (17) (2022) 10354–10363.
[44] R. Yang, D. Li, S.L. Salazar, Z. Rao, M. Ar\ic\i, W. Wei, Photothermal properties and photothermal conversion performance of nano-enhanced paraffin as a phase change thermal energy storage material, Sol. Energy Mater. Sol. Cells 219 (2021) 110792.
[45] R. Fan, M. Wan, N. Zheng, Z. Sun, Simultaneously enhanced light absorption and heat transfer capability of melamine foam stabilized phase change composites by carbon black and metal fins for photothermal conversion and storage, J. Energy Storage 54 (July) (2022) 105278, https://doi.org/10.1016/j.est.2022.105278.
[46] Y. Zhang, M.M. Umair, S. Zhang, B. Tang, Phase change materials for electron-triggered energy conversion and storage: a review, J. Mater. Chem. A 7 (39) (2019) 22218–22228.
[47] Y. Lin, Y. Jia, G. Alva, and G. Fang, "Review on thermal conductivity enhancement, thermal properties and applications of phase change materials in thermal energy storage," vol. 82, no. May 2017, pp. 2730–2742, 2018.
[48] X. Cui, et al., Photothermal Nanomaterials: a Powerful Light-to-Heat Converter, Chem. Rev. 123 (11) (2023) 6891–6952, https://doi.org/10.1021/acs.chemrev.3c00159.
[49] V. Georgakilas, J.A. Perman, J. Tucek, R. Zboril, Broad family of carbon nanoallotropes: classification, chemistry, and applications of fullerenes, carbon dots, nanotubes, graphene, nanodiamonds, and combined superstructures, Chem. Rev. 115 (11) (2015) 4744–4822.
[50] X. Zuo, et al., Lauric acid/expanded graphite composite phase change film with high thermal conductivity for thermal management, Energy Fuels 38 (3) (2024) 2480–2488.
[51] Y.-J. Huo, T. Yan, S.-F. Wu, Z.-H. Kuai, W.-G. Pan, Preparation and thermal properties of palmitic acid/copper foam phase change materials, Energy 293 (2024) 130629.
[52] S.K. Sahoo, M.K. Das, P. Rath, Application of TCE-PCM Based Heat Sinks for Cooling of Electronic Components: A Review, 59, Elsevier, 2016.
[53] S.B. Oskouei, Z.-R. Li, Ö. Bayer, L.-W. Fan, Close-contact melting and natural convection in unconstrained melting: a parametric study, Int. J. Heat. Mass Transf. 218 (2024) 124795.
[54] N. Hu, Z.-R. Li, Z.-W. Xu, L.-W. Fan, Rapid charging for latent heat thermal energy storage: a state-of-the-art review of close-contact melting, Renew. Sustain. Energy Rev. 155 (2022) 111918.
[55] W. Fu, X. Yan, Y. Gurumukhi, V.S. Garimella, W.P. King, N. Miljkovic, High power and energy density dynamic phase change materials using pressure-enhanced close contact melting, Nat. Energy 7 (3) (2022) 270–280, https://doi.org/10.1038/s41560-022-00986-y.
[56] T. Shockner, G. Ziskind, Experimental and numerical evaluation of phase-change material performance in a vertical cylindrical capsule for thermal energy storage, Appl. Therm. Eng. 219 (2023) 119519.
[57] H. Deng, S. Hong, Z. He, and Z. Wu, "Temperature response and liquid film morphology of dynamic phase change materials under constant and periodic heating scenarios," Int. J. Heat. Mass Transf., vol. 247, p. 127196, doi: 10.1016/j.ijheatmasstransfer.2025.127196.
[58] Z.-R. Li, Z.-K. Zhang, X.-R. Wang, S.-S. Ni, L.-W. Fan, Synergistic enhancement strategy on the heat charging process of a shell-and-tube thermal storage device based on close-contact melting mechanism and nano-enhanced phase change material, J. Energy Storage 72 (2023) 108529.
[59] A. Palacios, L. Cong, M.E. Navarro, Y. Ding, C. Barreneche, Thermal conductivity measurement techniques for characterizing thermal energy storage materials – A review, Renew. Sustain. Energy Rev. 108 (March) (2019) 32–52, https://doi.org/10.1016/j.rser.2019.03.020.
[60] Z. Chen, F. Shan, L. Cao, G. Fang, Synthesis and thermal properties of shape-stabilized lauric acid/activated carbon composites as phase change materials for thermal energy storage, Sol. Energy Mater. Sol. Cells 102 (2012) 131–136, https://doi.org/10.1016/j.solmat.2012.03.013.
[61] G. Zhang, Y. Sun, C. Wu, X. Yan, W. Zhao, C. Peng, Low-cost and highly thermally conductive lauric acid–paraffin–expanded graphite multifunctional composite phase change materials for quenching thermal runaway of lithium-ion battery, Energy Rep. 9 (2023) 2538–2547, https://doi.org/10.1016/j.egyr.2023.01.102.
[62] G.U. Maheswararao, D.J. Krishna, Measurement of thermophysical properties of some potential organic PCMs for low-temperature thermal energy storage systems, ISME J. Therm. Fluids 4 (02) (2018) 18–28.
[63] R.M. Saeed, J.P. Schlegel, C. Castano, R. Sawafta, V. Kuturu, Preparation and thermal performance of methyl palmitate and lauric acid eutectic mixture as phase change material (PCM), J. Energy Storage 13 (2017) 418–424, https://doi.org/10.1016/j.est.2017.08.005.
[64] S. Harish, D. Orejon, Y. Takata, M. Kohno, Thermal conductivity enhancement of lauric acid phase change nanocomposite with graphene nanoplatelets, Appl. Therm. Eng. 80 (2015) 205–211, https://doi.org/10.1016/j.applthermaleng.2015.01.056.
[65] B. Kalidasan, A.K. Pandey, S. Rahman, A. Yadav, M. Samykano, V.V. Tyagi, Graphene–Silver Hybrid Nanoparticle based Organic Phase Change Materials for Enhanced Thermal Energy Storage, Sustain 14 (20) (2022) 1–16, https://doi.org/10.3390/su142013240.
[66] R. K. R, M. Samykano, A.K. Pandey, K. Kadirgama, V.V. Tyagi, A comparative study on thermophysical properties of functionalized and non-functionalized Multi-Walled Carbon Nano Tubes (MWCNTs) enhanced salt hydrate phase change material, Sol. Energy Mater. Sol. Cells 240 (March) (2022) 111697, https://doi.org/10.1016/j.solmat.2022.111697.
[67] B. Kalidasan, A.K. Pandey, R. Saidur, B. Aljafari, T. Kareri, Expanded graphite intersperse reliable binary eutectic phase change material for low temperature thermal regulation systems, Mater. Today Sustain. 24 (5) (2023) 1–14, https://doi.org/10.1016/j.mtsust.2023.100602.
[68] A.K. Mishra, B.B. Lahiri, V. Solomon, J. Philip, Nano-inclusion aided thermal conductivity enhancement in palmitic acid/di-methyl formamide phase change material for latent heat thermal energy storage, Thermochim. Acta 678 (June) (2019) 178309, https://doi.org/10.1016/j.tca.2019.178309.
[69] T.Lo Wong, C. Vallés, A. Nasser, C. Abeykoon, A critical experimental evaluation of hexagonal boron nitride, graphene oxide and graphite as thermally conductive fillers in organic PCMs, J. Energy Storage 72 (2023) 108523, https://doi.org/10.1016/j.est.2023.108523. PD.
[70] P. Zhang, Y. Wang, Y. Qiu, H. Yan, Z. Wang, Q. Li, Novel composite phase change materials supported by oriented carbon fibers for solar thermal energy conversion and storage, Appl. Energy 358 (2024) 122546.
[71] J. Sobczak, et al., Thermophysical profile of ethylene glycol based nanofluids containing two types of carbon black nanoparticles with different specific surface areas, J. Mol. Liq. 326 (2021) 115255.
[72] K. Elsaid, et al., Thermophysical properties of graphene-based nanofluids, Int. J. Thermofluids 10 (2021) 100073.
[73] H. Waqas, et al., Enhancing the performance of thermal energy storage by adding nano-particles with paraffin phase change materials, Nanotechnol. Rev. 13 (1) (2024) 20230180.
[74] Y. Hu, Y. He, Z. Zhang, D. Wen, Enhanced heat capacity of binary nitrate eutectic salt-silica nanofluid for solar energy storage, Sol. Energy Mater. Sol. Cells 192 (2019) 94–102.
[75] M. Amin, N. Putra, E.A. Kosasih, E. Prawiro, R.A. Luanto, T.M.I. Mahlia, Thermal properties of beeswax/graphene phase change material as energy storage for building applications, Appl. Therm. Eng. 112 (2017) 273–280.
[76] N. Radhakrishnan, C.B. Sobhan, Thermophysical characterization and melting heat transfer analysis of an organic phase change material dispersed with GNP-Ag hybrid nanoparticles, Heat Mass Transf. Stoffuebertrag. 58 (10) (2022) 1811–1828, https://doi.org/10.1007/s00231-022-03218-x.
[77] J.-S. Yang, C.-L. Yang, M.-S. Wang, B.-D. Chen, X.-G. Ma, Crystallization of alkane melts induced by carbon nanotubes and graphene nanosheets: a molecular dynamics simulation study, Phys. Chem. Chem. Phys. 13 (34) (2011) 15476–15482.
[78] M.R. Zakaria, M.H. Abdul Kudus, H.Md. Akil, M.Z. Mohd Thirmizir, Comparative study of graphene nanoparticle and multiwall carbon nanotube filled epoxy nanocomposites based on mechanical, thermal and dielectric properties, Compos. Part B Eng. 119 (2017) 57–66, https://doi.org/10.1016/j.compositesb.2017.03.023.
[79] S.A. Angayarkanni, J. Philip, Review on thermal properties of nanofluids: recent developments, Adv. Colloid. Interface Sci. 225 (2015) 146–176, https://doi.org/10.1016/j.cis.2015.08.014.
[80] V. Soni, Nanoadditive Particles segregation and mobility in phase change materials, Int. J. Heat. Mass Transf. 165 (2021) 120676.
[81] X. Fang, et al., Increased thermal conductivity of eicosane-based composite phase change materials in the presence of graphene nanoplatelets, Energy Fuels 27 (7) (2013) 4041–4047, https://doi.org/10.1021/ef400702a.
[82] R.J. Warzoha, R.M. Weigand, A.S. Fleischer, Temperature-dependent thermal properties of a paraffin phase change material embedded with herringbone style graphite nanofibers, Appl. Energy 137 (2015) 716–725, https://doi.org/10.1016/j.apenergy.2014.03.091.
[83] Y. Anggraini, A. Yusuf, S. Viridi, D. Kurnia, S. Wonorahardjo, I.M. Sutjahja, Magnetic dopant and field effects on the heat discharge of organic PCM based lauric acid, Exp. Therm. Fluid. Sci. 152 (June 2023) 2024, https://doi.org/10.1016/j.expthermflusci.2023.111105.
[84] X. Sun, L. Liu, Y. Mo, J. Li, C. Li, Enhanced thermal energy storage of a paraffin-based phase change material (PCM) using nano carbons, Appl. Therm. Eng. 181 (August) (2020), https://doi.org/10.1016/j.applthermaleng.2020.115992.
[85] R.K. Kittusamy, V. Rajagopal, P.G. Felix, Numerical and experimental investigation on the melting heat transfer of nanographene-enhanced phase change material composites for thermal energy storage applications, Int. J. Heat. Mass Transf. 206 (2023) 123940.
[86] D. Cabaleiro, S. Hamze, J. Fal, M.A. Marcos, P. Estellé, G. Żyła, Thermal and physical characterization of PEG phase change materials enhanced by carbon-based nanoparticles, Nanomaterials 10 (6) (2020) 1–24, https://doi.org/10.3390/nano10061168.
[87] Y. Wang, B. Tang, S. Zhang, Single-walled carbon nanotube/phase change material composites: sunlight-driven, reversible, form-stable phase transitions for solar thermal energy storage, Adv. Funct. Mater. 23 (35) (2013) 4354–4360, https://doi.org/10.1002/adfm.201203728.
[88] A.M. Elbasiony, et al., Tailoring the linear and nonlinear optical properties of PVC/PE blend polymer by insertion the spindle copper nanoparticles, Opt. Mater. (Amst) 148 (2024) 114811.
[89] D. Han, Z. Meng, D. Wu, C. Zhang, H. Zhu, Thermal properties of carbon black aqueous nanofluids for solar absorption, Nanoscale Res. Lett. 6 (2011) 1–7, https://doi.org/10.1186/1556-276X-6-457.

[90] Y. Chen, et al., Enhanced light-to-thermal conversion performance of self-assembly carbon nanotube/graphene-interconnected phase change materials for thermal-electric device, J. Energy Storage 72 (2023) 108387.
[91] L. Yang, Y. Yuan, N. Zhang, Y. Dong, Y. Sun, W. Ji, Photo-to-thermal conversion and energy storage of lauric acid/expanded graphite composite phase change materials, Int. J. Energy Res. 44 (11) (2020) 8555–8566.
[92] D.K. Lee, S. Jeon, J. Jeong, K.S. Song, W.S. Cho, Carbon nanomaterial-derived lung burden analysis using UV–Vis spectrophotometry and proteinase K digestion, Part Fibre Toxicol. 17 (1) (2020) 1–11, https://doi.org/10.1186/s12989-020-00377-9.
[93] S. Zhang, et al., Effect of the irradiation intensity on the photo-thermal conversion performance of composite phase change materials: an experimental approach, Renew. Energy 225 (2024) 120284.
[94] P. Zhang, Y. Qiu, C. Ye, Q. Li, Anisotropically conductive phase change composites enabled by aligned continuous carbon fibers for full-spectrum solar thermal energy harvesting, Chem. Eng. J. 461 (2023) 141940.
[95] Q. Xin, et al., Antibacterial carbon-based nanomaterials, Adv. Mater. 31 (45) (2019) 1804838.
[96] L. Zhang, L. Chen, J. Liu, X. Fang, Z. Zhang, Effect of morphology of carbon nanomaterials on thermo-physical characteristics, optical properties and photo-thermal conversion performance of nanofluids, Renew. Energy 99 (2016) 888–897, https://doi.org/10.1016/j.renene.2016.07.073.
[97] Y.A. Bhutto, A.K. Pandey, R. Saidur, I.A. Laghari, D. Buddhi, V.V. Tyagi, Investigating the optical absorption and thermal conductivity of nano-enhanced lauric acid phase change material for energy storage application, IOP Conf. Ser.: Earth Environ. Sci. 1281 (1) (2023) 12013.
[98] B. Mu, M. Li, Synthesis of novel form-stable composite phase change materials with modified graphene aerogel for solar energy conversion and storage, Sol. Energy Mater. Sol. Cells 191 (2019) 466–475.
[99] S. Pugalenthi, M. Chellapandian, J.J.J. Dharmaraj, J. Devaraj, N. Arunachelam, S. B. Singh, Enhancing the thermal transport property of eutectic lauric-stearic acid based phase change material with silicon carbide nanoparticles for usage in battery thermal management system, J. Energy Storage 84 (2024) 110890.
[100] Q. Tan, H. Liu, Y. Shi, M. Zhang, B. Yu, Y. Zhang, Lauric acid/stearic acid/nano-particles composite phase change materials for energy storage in buildings, J. Energy Storage 76 (2024) 109664.
[101] Y.A. Bhutto, A.K. Pandey, R. Saidur, P.K.S. Rathore, M. Samykano, Hybrid silver-graphene nanoparticles enhanced Lauric Acid phase change material for photovoltaic and thermoelectric generator applications: experimental and simulation analysis, J. Energy Storage 93 (2024) 112320.
[102] A. Sar\i, A. Karaipekli, C. Alkan, Preparation, characterization and thermal properties of lauric acid/expanded perlite as novel form-stable composite phase change material, Chem. Eng. J. 155 (3) (2009) 899–904.
[103] S. Harish, D. Orejon, Y. Takata, M. Kohno, Thermal conductivity enhancement of lauric acid phase change nanocomposite in solid and liquid state with single-walled carbon nanohorn inclusions, Thermochim. Acta 600 (2015) 1–6.
[104] Y. Zhang, et al., Paraffin wax with an addition of nano Ti2O3: improve thermal and photothermal performances with little decreased latent heat, Sol. Energy 246 (2022) 273–280.
[105] X. Luo, B. Hao, H. Xiang, H. Li, Z. Tao, A novel phase change materials used for direct photothermal conversion and efficient thermal storage, Sol. Energy Mater. Sol. Cells 251 (2023) 112142.
[106] X. Zou, J. Liu, Polyoxyethylene based phase change materials with enhanced mechanical property, thermal conductivity and photo-thermal energy charging capacity, Energy Rep. 6 (2020) 2948–2955.
[107] M. Ouikhalfan, A. Sar\i, G. Hekimo\uglu, O. Gencel, V.V. Tyagi, Thermal energy storage properties, thermal conductivity, chemical/and thermal reliability of three different organic phase change materials doped with hexagonal boron nitride, Surf. Interfaces. 32 (2022) 102176.
[108] W. Yang, et al., Biobased photothermal responsive shape memory Polythioether/MXene nanocomposites with self-extinguishing performance, Chem. Eng. J. (2024) 154591.
[109] D. Han, Z. Meng, D. Wu, C. Zhang, H. Zhu, Thermal properties of carbon black aqueous nanofluids for solar absorption, Nanoscale Res. Lett. 6 (1) (2011) 1–7, https://doi.org/10.1186/1556-276X-6-457.
[110] C. Wu, et al., Highly efficient solar-thermal-electric conversion based on asymmetric binary-architecture design in solid-solid composite phase change materials, Compos. Part a Appl. Sci. Manuf. 181 (February) (2024), https://doi.org/10.1016/j.compositesa.2024.108170.
[111] J. Hu, Z. Wei, B. Ge, L. Zhao, K. Peng, Z. Shi, AlN micro-honeycomb reinforced stearic acid-based phase-change composites with high thermal conductivity for solar-thermal-electric conversion, J. Mater. Chem. A 11 (20) (2023) 10727–10737, https://doi.org/10.1039/d2ta08748k.